MODELING THE GROWTH AND DISSOLUTION OF CLOTS

IN FLOWING BLOOD

A Dissertation

by

ANAND MOHAN

Submitted to the Office of Graduate Studies of
Texas A&M University
in partial fulfillment of the requirements for the degree of

DOCTOR OF PHILOSOPHY

August 2005

Major Subject: Mechanical Engineering

MODELING THE GROWTH AND DISSOLUTION OF CLOTS

IN FLOWING BLOOD

A Dissertation

by

ANAND MOHAN

Submitted to the Office of Graduate Studies of
Texas A&M University
in partial fulfillment of the requirements for the degree of

DOCTOR OF PHILOSOPHY

Approved by:

Chair of Committee,	K. R. Rajagopal
Committee Members,	J. R. Walton
	J. D. Humphrey
	N. K. Anand
	R. Lazarov
Head of Department,	D. O'Neal

August 2005

Major Subject: Mechanical Engineering

ABSTRACT

Modeling the Growth and Dissolution of Clots

in Flowing Blood. (August 2005)

Anand Mohan, B.Tech., Indian Insitute of Technology, Madras;

M.S., Texas A&M University

Chair of Advisory Committee: Dr. K. R. Rajagopal

Multiple interacting mechanisms control the formation and dissolution of clots to maintain blood in a state of delicate balance. In addition to a myriad of biochemical reactions, rheological factors also play a crucial role in modulating the response of blood to external stimuli. The broad stimuli for clot formation were laid out, more than a century ago, in, what is now referred to as, Virchow's triad. To date, a comprehensive model for clot formation and dissolution, that takes into account the biochemical, medical and rheological factors, has not been put into place, the existing models emphasizing either one or the other of the factors. In this dissertation, a model is developed for clot formation and dissolution that incorporates many of the relevant crucial factors that have a bearing on the problem. The model, though just a first step towards understanding a complex phenomenon goes further than previous models in integrating the biochemical, medical and rheological factors that come into play. The model is tested in some simple flow situations as part of an attempt to elucidate Virchow's triad. Extensions to the model, along with detailed numerical studies, will hopefully aid in a clearer understanding of the phenomenon, and in making relevant clinical correlations.

To My Mentors : past, present, future

ACKNOWLEDGMENTS

I thank Professor Rajagopal for gardening with great skill and care; with his dedicated attention, out of seeds sown by Dr. D. Veeraraghavan, Dr. M. Antony Reddy, and Dr. (MBBS) Clement Reddy, something of value has emerged.

I profited immensely from the teachers, relatives, more than friends, friends, and fascinating acquaintances whose paths, by fortuitous chance, wound through College Station in the last six years. My first semester was especially crucial for the several interactions with Professors Rajagopal, Walton, and Humphrey, who emphasized the cultivation of a scientific temper and the nurturing of a love for learning. Through various conversations, both within and without the classroom, Professors Anand and Lazarov fed my fledgling enthusiasm for knowledge, and I finally beaked out of my shell under Professor Harris' (of the Department of Biochemistry and Biophysics) tutorship. My aunts (Dr. Chitra Subramanian, and Mrs. Anuradha Sudharsan) and uncles (Dr. Ramachandran Muralidhar, and Mr. Arunachalam Sudharsan) were instrumental in giving support and in offering insightful, and thought-provoking, questions; this dissertation would be far poorer without their encouragement. Thanks to Dr. Luoyi Tao for his kind natured assistance and sage counsel, and to Aravind Nayak (currently employed with Agere systems) whose comforting words led me out of moments of withdrawal, self-laceration, and despair. My friends, Krishna Kannan, Parag Ravindran, Saravanan Umakanthan, Sharat Prasad, C. S. Shankar Ram, H. Pradeep, Waqar Malik, Ronald Bridges, V. N. Shankar, and Chris Bowlin brought cheer and chattering camaraderie to long hours at the laboratory; they will be missed along with several others, not named but not forgotten, who graduated from Texas A&M long ago. This vote of thanks would remain incomplete without acknowledging some eye-opening encounters with Professor M. S. Ananth, Professor V. Girault,

and Mr. Govindarajan Thirumalai (currently employed with Yahoo! India), and the guidance and professional help from Dr. M. Ramakrishna, Dr. J. Murali Krishnan, and Dr. Keshava Rajagopal. Several others have contributed in their own way to this work (the National Energy Technology Laboratory of the US Department of Energy that provided financial support through the University Partnership Program, being among them), and their names would be mentioned here if not for the lapses of memory.

Finally, and most importantly, I thank my wonderful mother (Usha), my loving father (Mohan Seshadri), and my affectionate brother (Harish): this dissertation is my humble tribute to what, in infinite patience, they have given and sacrificed.

TABLE OF CONTENTS

LIST OF TABLES

LIST OF FIGURES

CHAPTER I

THE PHENOMENON OF HEMOSTASIS, ITS CLINICAL RELEVANCE, AND

THE ROLE OF MATHEMATICAL MODELING

The human body is fascinating for its complexity and the surprising ease with which it maintains itself in a dynamic equilibrium (a process known as homeostasis) conducive to the preservation of life. One among many interacting systems, the cardiovascular system, consisting in the heart and the vascular network of arteries, arterioles, capillaries, venules and veins, is responsible for the circulation of blood, supplying nutrition and oxygen to, and removing the byproducts of metabolism (nitrogenous wastes, carbon dioxide) from, the trillions of cells in the body.

Blood, sometimes refered to as 'the river of life', consists in 'cell' matter (the formed elements : red blood cells (RBCs), white blood cells (WBCs), platelets) in an aqueous plasma solution. Plasma consists primarily of water in which various proteins (fibrinogen, prothrombin, etc.) are dissolved along with ions (calcium (Ca^{2+}), chloride (Cl^-), etc.). The vascular network branches into smaller vessels as oxygenated blood flows away from the heart, and the thickness of the vessel walls decreases as well; subsequently, there is a consolidation in vessel size as deoxygenated blood flows back toward the heart. The walls of the large vessels (arteries and veins, between 0.1 mm and 30 mm in diameter) consist in three layers (the intima, the media and the adventitia) whose thickness and composition vary along the entire vascular network [46]. The intima consists of the endothelium that is in contact with blood, and the subendothelial layer beneath that consists in several proteins (von Willebrand Factor, collagen, etc.). The intima is separated from the media by a layer of elastin (a

---

The journal model is *Interfaces and Free Boundaries.*

structural protein), the internal elastic lamina. The media consists mainly of smooth muscle cells and the matrix of proteins these cells secrete and maintains the structural integrity of the vessel, while the adventitia forms the outer layer between the vessel and the surrounding tissue. The walls of the smaller vessels (arterioles, capillaries and venules, less than 0.1 mm in diameter) consist primarily of the endothelial cell layer, and a layer of pericytes beneath that are embedded in a matrix that contains smooth muscle cells and the proteins secreted by both these cell types [50].

A. Hemostasis and Virchow's triad

Numerous mechanisms have evolved to maintain blood in a state of delicate balance. Factors and processes exist both to promote and inhibit clot formation, as well as, clot maintenance. A fluid tissue under normal conditions, blood coagulates due to an imbalance in favor of pro-thrombotic factors. In turn, clot maintenance is determined by various stimuli like vessel wall injury, endothelial dysfunction, abnormally high shear stresses, flow recirculation and stasis, etc. Under normal circumstances, the process of clot formation, or hemostasis, is designed to seal defects in the cardiovascular system and stem hemorrhage as part of a physiological response that precedes healing. The eminent pathologist Rudolf Virchow, well over a century ago [113], laid out the broad stimuli for thrombus formation : 1. local flow stasis/stagnation, 2. blood vessel injury/endothelial dysfunction, 3. "Hypercoagulability" or an augmented native tendency for blood to clot. This basic picture, or what is refered to as Virchow's triad, has been fleshed out with the greater details that have emerged in the years since. The current understanding is that the endothelium plays a key role in maintaining blood fluidity by balancing a natural tendency to clot in isolation with a set of counteracting mechanisms (secretion of thrombomodulin, release of nitric oxide and

PGI_2 etc.). When the endothelium is disrupted, blood comes into contact with proteins embedded in the subendothelial layers, and this initiates the formation of a clot. Platelet activation and subsequent adhesion to the subendothelial surface is accompanied by platelet aggregation. Simultaneously, the extrinsic pathway of coagulation (and the intrinsic pathway, although f-XII is not relevant in the in-vivo setting [37]), particularly active in the setting of tissue damage, leads to the formation of thrombin, and hence the cleavage of fibrinogen to form fibrin monomers that polymerize to form fibrin strands. Fibrinolysis, the process leading to the degradation of fibrin molecules is signalled almost simulatneously with clot formation, and leads to the dissolution of the clot. The entire process is host to multiple interacting mechanisms that are carefully controlled so as to heal vascular injury and stem blood loss, with only transient or no resultant tissue ischemia. In addition, rheological factors also play a crucial role [43],[62],[110] in modulating the response at each level.

Typically, clot formation occurs only if the hemostatic stimuli reach a certain threshold; this threshold is conditioned by both hemodynamic and biochemical factors including flow conditions, availability of membrane binding sites for catalysis, concentration of di/multivalent ions like calcium (Ca^{2+}), and, finally, concentrations of the reagents involved in clot formation: platelets and coagulation factors. It is apt to think of the mechanisms of hemostasis as being in a state of "system idling" due to subthreshold stimuli, which is primed to respond explosively once this threshold is crossed. During hemostasis, the system responds in a manner that will eventually return it to its idling state while at the same time redressing the initial stimulus. Pathological conditions may result as a consequence of either hypo- or hyper function of any or all of the components of the mechanisms of hemostasis. On the one hand, hypofunction of these components results in impairments in clot function or maintenance, i.e., bleeding disorders. On the other hand, hyperfunction of these

functions results in inappropriate clot formation or maintenance, i.e., thrombotic or thromboembolic disorders.

B. Clinical relevance

Disorders in thrombus formation or destruction govern several diseases, either wholly or substantially, and the morbidity and mortality of such diseases is of significant importance. Most of the common pathologies of the cardiovascular system result in deleterious consequences, in large part, due to abnormalities of coagulation. Collectively, these diseases are the leading cause of death in the developed world. It is useful to classify patients into those with disorders of pathologic thrombus formation and maintenance and conversely, those with disorders characterized by impaired thrombus formation/maintenance (see [2] for a detailed review).

The first set of patients are organized anatomically based on the sites of pathologic thrombus or thromboembolus. This is done because the clinical manifestation of these diseases and often the requisite therapies are governed by the site of thrombus/thromboembolus. Treatment of atrial thrombosis, for instance, centers on rate control whereas artificial device technology in the form of Ventricular Assist Devices (VADs) represents a modality in the treatment of ventricular thrombosis. Valvular thrombosis is mostly a problem with artificial mechanical valves, but occurs, in rare instances, on native valves, and is treated by anti-coagulation regimens. Arterial thrombosis (acute coronary syndromes (ACS), and extremity arterial insufficiency being two common and important examples; Figure 1 shows a picture of corononary thrombosis where a thrombus occludes the coronary artery) is again treated very differently, with the focus being on revascularization and concomitant anticoagulation. The pathogenesis of Deep Venous Thrombi (DVT), with or without resultant pul-

monary thrombo-embolism (PE), is understood within the framework of Virchow's triad. A myriad of hypercoagulable states (either Inherited or Acquired; see [9]) increase the risk of DVT formation, and while hereditary factors contribute to the risk of inherited hypercoagulable states, hemodynamics plays a role in the acquired states (especially post-surgical patients and postpartum patients, who are often in a minimally ambulatory state). Endothelial dysfunction is also a risk factor for DVT formation. Treatmentof DVT/PE typically focuses on anticoagulation regimes, and, in some cases, placement of vena caval filters.

The second set of patients, in contrast, are organized based on the defective hemostatic system component(s). This is because these diseases, while differing with regards to etiology and pathogenesis, all manifest as bleeding disorders. These disorders all have in common either inadequate levels of components in the hemostatic system or dysfunction of these components. Treatment generally involves simple replacement of deficient/defective components, or in some cases, pharmacologic enhancement of hemostatic system function. Broadly, treatment approaches involve: 1. blood product administration and, 2. pharmacologic agents that augment platelet function, coagulation factor function, or inhibit fibrinolysis.

The diagnosis of clinically relevant risk factors in patients presenting with either pathologic thrombosis or bleeding disorders is of utmost importance in guiding the management and treatment of the pathology. Laboratory evaluations involving global tests of the hemostatic system (like the Prothrombin time (PT) and activated Partial Thromboplastin Time (PTT) tests), and, if abnormal results ensue, a second tier of tests either to determine specific biologic risk factors (in the cases where an inherited hypercoagulable state is suspected; such tests involve immunologic and functional assays [9]) or to determine factor deficiencies, fibrinogen levels, von Willebrand disease, etc. (in the cases where bleeding disorders are manifest; such tests involve repeat-
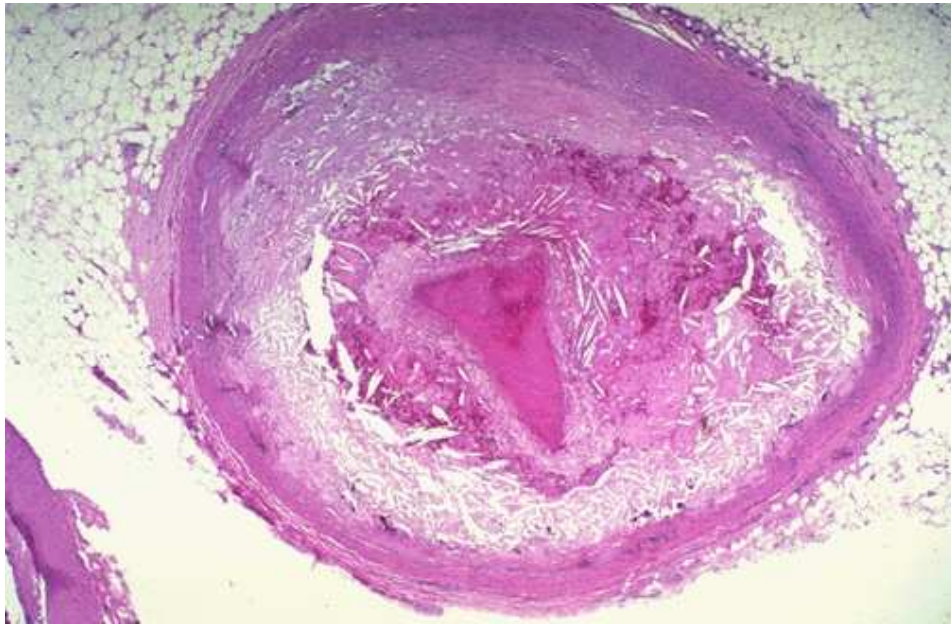
Fig. 1. Coronary thrombosis: A thrombus occludes the lumen of the coronary artery;
Source : www-medlib.med.utah.edu

ing the PT and PTT after mixing the patient's plasma with normal plasma and a slew of chemical, immunochemical procedures [88]) form an important part of such diagnosis. Mathematical modeling (theoretical modeling along with computational methods) has emerged as a useful tool that can be used to complement such laboratory evaluations and thus aid in confirming or even interpreting the results from a laboratory evaluation. In addition, mathematical modeling helps in supplementing experimental data and hence in forming a clearer picture of the hemostatic system.

C. The role of mathematical modeling

Constitutive modeling of blood has assumed increased importance with the realization that the flow characteristics of blood influence the etiology and pathogenesis of several cardiovascular diseases (for instance, in the stenosis of the coronary arteries

due to thrombosis over atherosclerotic plaques, and in the possible embolism of such thrombi). The development and testing of artificial devices used in the treatment of ventricular thrombosis requires accurate, yet simple, models for describing blood flow that can be used for computational simulations in such complex geometries (see [16]). Such models have emerged in the recent past, though none of these models has integrated all aspects of the rheological behavior of blood in a single unifying framework.

Mathematical modeling of the hemostatic mechanism has become increasingly important in recent years as a useful supplement to experimental data, and as a means for systematically quantifying the various biochemical factors involved in the formation and dissolution of clots. A mathematical model of the in-vitro formation and dissolution of clots would be especially useful in confirming or even interpreting the results from laboratory tests like the PT and the aPTT. Although many mathematical models have been posited for various sets of reactions that are involved in the enzyme cascade of coagulation, none has been developed that puts together the entire sequence of events from clot formation till dissolution (i.e. platelet activation, coagulation, *and* fibrinolysis). Such a model, once corroborated with existing experimental data, would be of immense value in making predictions with clear clinical correlations.

Constitutive modeling of (the various types of) clots is of importance when one tries to understand the role of flow and shear stresses during clot formation and rupture. Development of models predictive of clot mechanical behavior, will allow for testing of the effects of various biochemical and local hemodynamic alterations on thrombus hemostatic function. A rheological model of clot formation can also be used to generate tissue sealants or biological "glues (used, in the clinical setting, to effect optimal hemostasis) with ideal biochemical compositions and resultant mechanical

properties. Reliable rheological models for clots are sparse in the literature, apart from being largely simplified at present, and a rigorous model that could be used in three-dimensional flow situations where clot formation is suspected, or encountered, would be of importance.

A set of models that could be used to predict regions susceptible to clot formation, track the extent of clotting, once initiated, and, if applicable, predict its dissolution or an embolism would be of immense value to engineers seeking to minimize such an occurence within a cardiovascular device. There is a need to develop models that can help us understand the interplay of the rheological and biochemical factors under the diverse flow conditions found in the human vasculature. Such models are in their infancy at present, tending to focus on single aspects of this multifaceted problem, and an integrated model is yet to emerge that incorporates all these factors in a physiologically accurate scheme.

D.   Specific aims of dissertation and organization

In this dissertation, a framework is developed for the elucidation of Virchow's triad; each component of this framework is corroborated with the appropriate experimental data and their predictions checked for reliability and clinical relevance. The entire framework is tested in some simple flow problems, and the results from these calculations are discussed.

A model is developed for describing the flow of human blood; the model is capable of describing the shear-thinning and viscoelastic fluid-like behavior (with a deformation-dependent relaxation time) of blood, and arises in a thermodynamic setting that recognises that viscoelastic fluids possess multiple natural configurations. The model is corroborated with data for apparent viscosity, and oscillatory flow in

small diameter tubes. The model predictions for flow reversals when blood is subject to pulsatile pressure gradients in a rigid-walled pipe tie in nicely with observations on the deformation-dependent viscoelastic behavior of blood, and the model predictions of negligible first normal stress differences tie in with experimental observations.

A mathematical model consisting in a set of convection-diffusion-reaction equations is used to simulate the transport and the biochemical changes in flowing human blood of the various reactants involved in platelet activation, (the extrinsic and intrinsic pathways of) coagulation, and fibrinolysis. The growth and dissolution of the clot that is formed is governed by the boundary conditions that govern the surface concentration of TF-VIIa, the generation of XIa via the intrinsic pathhway, the extent of platelet-subendothelium interaction, and the secretion of tPA due to endothelial activation. The model is corroborated with data for clot formation, and for clot dissolution, in quiescent human plasma (this involves only the reaction-diffusion equations), and its predictions for the severity of Antithrombin-III deficiency over Protein-C deficiency offer an insight into clinical observations.

A model is developed for describing the flow of a certain kind of clot formed from human plasma that is most likely to occur under normal physiological conditions; the model is capable of describing the viscoelastic-fluid like behavior of the clot, and its predictions for the apparent viscosity that would be inferred from the clot are in keeping with the physical expectation that the clot be more viscous than the plasma from which it is formed.

The framework of models is applied to three simple flow problems that are representative of some conditions encountered in the vasculature, and the results from the solution of two of these problems are analyzed. The results for clot formation and dissolution in quiescent plasma on a thrombogenic plane are obtained. The equations for the case of time-varying poiseuille-type flow are developed but they are not

solved. A system of models consisting of two shear-thinning viscoelastic liquids and a simple activation criterion allowing a switch between the model for liquid prior to activation (Blood) and the liquid after activation (Clot: which is more viscous than blood) in the context of oscillatory flow in an infinitely long rigid-walled cylindrical pipe is studied, and the simulations reveal qualitative insights into the phenomenon of clot formation in flowing blood.

A model that accounts for the rheology of blood and the clot while at the same time incorporating the basic reactions of platelet activation, the extrinsic and intrinsic coagulation pathways, and fibrinolysis and allowing for surface modulation of these reactions is presented. Clot formation and dissolution in flowing blood is viewed as a moving boundary problem involving two viscoelastic liquids; the dynamics of the interface is governed by both mechanical and biochemical factors. This is but a first step in the direction of modeling and understanding the problem of clot formation and dissolution in flowing blood.

An accurate mathematical model requires a proper understanding of the myriad of factors that play a role in the formation and dissolution of clots, and hence the relevant rheological, biochemical, and medical issues are discussed (or appropriate references given) in some length at each stage in the assembly of the framework.

The key concepts (and the relevant mathematical notation) employed in the rest of this dissertation are outlined in Chapter 2. A shear-thinning viscoelastic fluid model with a deformation-dependent relaxation time for describing the flow of blood is developed, and tested in Chapter 3. A mathematical model for studying the formation and dissolution of clots is developed and tested (for quiescent plasma in the in-vitro setting) in Chapter 4. A viscoelastic fluid model for describing the flow of a particular type of plasma clot is developed and tested in Chapter 5. The results for clot formation and dissolution on a thrombogenic surface in quiescent plasma (in-

vitro) are reviewed, the equations relevant to time-varying poiseuille-type flow with clot formation in a cylindrical annular region are presented, and the entire framework of models is applied to some simple flow problems in Chapter 6; a summary of the results is given, and, in concluding, suggestions that could be taken up for future study are made.

CHAPTER II

PRELIMINARIES

The notation involved in the development of constitutive models for viscoelastic fluids (with multiple natural configurations) is reviewed. The notation is encountered when the models for describing the flow of blood and the flow of the plasma clot are presented. The form of the convection-diffusion-reaction equations that are used in the mathematical model for describing the formation and dissolution of clots in flowing blood is then outlined; these equations govern the movement and biochemical changes of the various constituents involved in hemostasis which are assumed to exist at every point in the domain whether the domain be occupied by blood or clot at any given instant in time. The balance equations encountered in applying the set of models to simple flow problems are then outlined.

A.   Constitutive models for viscoelastic fluids of the rate-type

The framework for the development of the constitutive theory for viscoelastic fluids (possessing multiple natural configurations) has been outlined in [81], and the notation introduced therein is adhered to here. Let $\kappa_R(B)$ and $\kappa_t(B)$ denote the reference and the current configuration of the body B at time t, respectively. Let $\kappa_{p(t)}(B)$ denote the stress-free configuration that is reached by instantaneously unloading the body which is at the configuration $\kappa_t(B)$ (Figure 2). As the body continues to deform these natural configurations $\kappa_{p(t)}(B)$ can change (the suffix p(t) is used in order to highlight that it is the preferred stress free state corresponding to the deformed configuration at time t. See Rajagopal [80] for a detailed discussion of the notion of natural configurations).

By the motion of a body we mean a one to one mapping that assigns to each
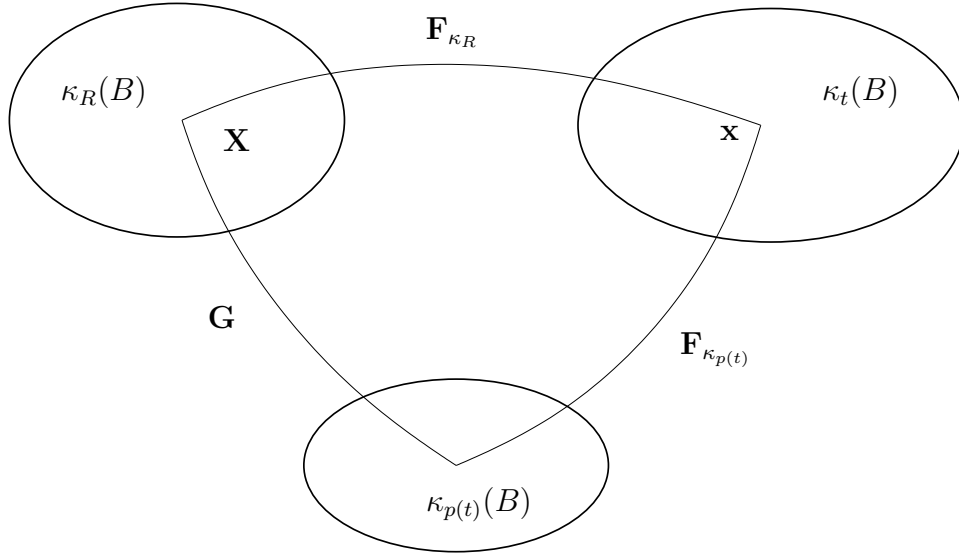
Fig. 2. Schematic of the natural configurations associated with a viscoelastic fluid having a single relaxation mechanism, and capable of instantaneous elastic response.

point $\mathbf{X} \in \kappa_R(B)$, a point $\mathbf{x} \in \kappa_t(B)$, for each t, i.e,

$$\mathbf{x} = \boldsymbol{\chi}_{\kappa_R}(\mathbf{X}_{\kappa_R}, t). \tag{2.1}$$

We assume that the motion is sufficiently smooth and invertible. We shall, for the sake of convenience, suppress B in the notation $\kappa_R(B)$, etc.

The deformation gradients, $\mathbf{F}_{\kappa_R}$, and the left and right Cauchy-Green stretch tensors, $\mathbf{B}_{\kappa_R}$ and $\mathbf{C}_{\kappa_R}$, are defined through:

$$\mathbf{F}_{\kappa_R} = \frac{\partial \boldsymbol{\chi}_{\kappa_R}}{\partial \mathbf{X}_{\kappa_R}} \;,\;\; \mathbf{B}_{\kappa_R} = \mathbf{F}_{\kappa_R}\mathbf{F}_{\kappa_R}^T, \text{ and } \mathbf{C}_{\kappa_R} = \mathbf{F}_{\kappa_R}^T\mathbf{F}_{\kappa_R} \;. \tag{2.2}$$

The left Cauchy-Green stretch tensor associated with the instantaneous elastic response from the natural configuration $\kappa_{p(t)}$ is defined in like fashion:

$$\mathbf{B}_{\kappa_{p(t)}} = \mathbf{F}_{\kappa_{p(t)}}\mathbf{F}_{\kappa_{p(t)}}^T \;. \tag{2.3}$$

The principal invariants of $\mathbf{B}_{\kappa_{p(t)}}$ are

$$\mathrm{I_B} = \mathtt{tr}(\mathbf{B}_{\kappa_{p(t)}}), \ \ \mathrm{II_B} = \frac{1}{2}\Big\{[\mathrm{tr}(\mathbf{B}_{\kappa_{p(t)}})]^2 - \mathrm{tr}(\mathbf{B}^2_{\kappa_{p(t)}})\Big\}, \ \text{and} \ \mathrm{III_B} = \det(\mathbf{B}_{\kappa_{p(t)}}) \ . \quad (2.4)$$

For homogeneous deformations, $\mathbf{F}_{\kappa_{p(t)}}$ denotes the deformation gradient between the natural configuration and the current configuration. The mapping $\mathbf{G}$ is defined through:

$$\mathbf{G} = \mathbf{F}_{\kappa_R \rightarrow \kappa_{p(t)}} = \mathbf{F}^{-1}_{\kappa_{p(t)}} \mathbf{F}_{\kappa_R} \ . \quad (2.5)$$

The velocity gradients, $\mathbf{L}$ and $\mathbf{L}_{\kappa_{p(t)}}$, are defined through

$$\mathbf{L} := \dot{\mathbf{F}}_{\kappa_R} \mathbf{F}^{-1}_{\kappa_R} \text{ and } \mathbf{L}_{\kappa_{p(t)}} = \dot{\mathbf{G}} \mathbf{G}^{-1} \ , \quad (2.6)$$

where the dot signifies the material time derivative.

The symmetric parts of $\mathbf{L}$ and $\mathbf{L}_{\kappa_{p(t)}}$, are defined through

$$\mathbf{D} = \frac{1}{2}(\mathbf{L} + \mathbf{L}^T) \text{ and } \mathbf{D}_{\kappa_{p(t)}} = \frac{1}{2}(\mathbf{L}_{\kappa_{p(t)}} + \mathbf{L}^T_{\kappa_{p(t)}}). \quad (2.7)$$

The upper convected Oldroyd derivative of $\mathbf{B}_{\kappa_{p(t)}}$, $\overset{\triangledown}{\mathbf{B}}_{\kappa_{p(t)}}$, is given through

$$\overset{\triangledown}{\mathbf{B}}_{\kappa_{p(t)}} = \dot{\mathbf{B}}_{\kappa_{p(t)}} - \mathbf{L}\mathbf{B}_{\kappa_{p(t)}} - \mathbf{B}_{\kappa_{p(t)}}\mathbf{L}^T = -2\mathbf{F}_{\kappa_{p(t)}} \mathbf{D}_{\kappa_{p(t)}} \mathbf{F}^T_{\kappa_{p(t)}} \ . \quad (2.8)$$

As we shall assume that the fluid (whether blood or plasma clot) is incompressible, we shall require that

$$\mathtt{tr}(\mathbf{D}) = 0 \ , \quad (2.9)$$

and

$$\mathtt{tr}(\mathbf{D}_{\kappa_{p(t)}}) = 0 \ . \quad (2.10)$$

1. Maximization of the rate of dissipation assumption

The procedure for obtaining models of the rate-type is outlined in [81], and models due to Maxwell, Oldroyd and Burgers are special models within this framework. The models arise in a thermodynamic setting that involves specifying the manner of the rate of dissipation and the manner in which energy is stored by the material in question. The procedure also guarantees constitutive relations that automatically meet the second law of thermodynamics.

The second law of thermodynamics is used in the following form:

$$\mathbf{T} \cdot \mathbf{D} - \rho \dot{\psi} - \rho \eta \dot{\theta} - \frac{\mathbf{q} \cdot \operatorname{grad}\theta}{\theta} = \rho \theta \zeta = \xi \ , \tag{2.11}$$

and $\zeta \geq 0$, or equivalently $\xi \geq 0$, is enforced. Here $\mathbf{T}$ is the stress tensor, $\mathbf{D}$ is the stretching tensor, ψ is the specific Helmholtz potential, η is the entropy, θ is the temperature, ζ is the rate of entropy production, and ξ is the rate of dissipation (which usually refers to the amount of working converted into "heat" or energy in thermal form).

The rate of dissipation is ensured to be non-negative, and the rate of dissipation is maximized to select the final constitutive equation. The salient feature of this approach is that we do not appeal to a procedure that is often used to place restrictions on allowable constitutive relations that presumes that the body can be subject to arbitrary processes (see [82] for a detailed discussion of these issues).

A brief sketch of the procedure to obtain the final constitutive equation, for a material subject to isothermal processes, is given below; further details are found in [81].

The rate of dissipation associated of the material, subject to isothermal processes,

is given by

$$\xi = \mathbf{T} \cdot \mathbf{D} - \dot{W} \ . \tag{2.12}$$

We make constitutive assumptions for the stored energy W, and rate of dissipation ξ for the material (a viscoelastic fluid), and assume that

$$W = \hat{W}(\mathrm{I_B}, \mathrm{II_B}) \ , \tag{2.13}$$

and

$$\xi = \hat{\xi}(\mathbf{B}_{\kappa_{p(t)}}, \mathbf{D}_{\kappa_{p(t)}}) \ . \tag{2.14}$$

We also stipulate that $\hat{\xi}(\cdot, \mathbf{0}) = 0$.

On differentiating Equation (2.13) with respect to time, we obtain

$$\dot{W} = \left(\alpha_0 \mathbf{1} + \alpha_1 \mathbf{B}_{\kappa_{p(t)}}\right) \cdot \dot{\mathbf{B}}_{\kappa_{p(t)}}, \tag{2.15}$$

where $\alpha_0 = (\frac{\partial \hat{W}}{\partial \mathrm{I_B}})$ and $\alpha_1 = 2(\frac{\partial \hat{W}}{\partial \mathrm{II_B}})$. It can now be shown that

$$\dot{W} = 2\left(\alpha_0 \mathbf{B}_{\kappa_{p(t)}} + \alpha_1 \mathbf{B}^2_{\kappa_{p(t)}}\right) \cdot \left(\mathbf{D} - \mathbf{D}_{\kappa_{p(t)}}\right) \ . \tag{2.16}$$

Substituting from Equation (2.16) in Equation (2.12), and using Equation (2.14) and the fact that only isochoric motions are allowed, we can stipulate the stress tensor as

$$\mathbf{T} = -p\mathbf{1} + 2\left(\alpha_0 \mathbf{B}_{\kappa_{p(t)}} + \alpha_1 \mathbf{B}^2_{\kappa_{p(t)}}\right) \ . \tag{2.17}$$

We also obtain that

$$\xi = \mathbf{T} \cdot \mathbf{D}_{\kappa_{p(t)}} \ . \tag{2.18}$$

The constrained maximization procedure involves extremizing ξ subject to constraints (Equations (2.10) and (2.18)), leading to the following equation for $\mathbf{D}_{\kappa_{p(t)}}$:

$$\mathbf{T} - \lambda_1 \frac{\partial \hat{\xi}}{\partial \mathbf{D}_{\kappa_{p(t)}}} - \lambda_2 \mathbf{1} = \mathbf{0} \ , \tag{2.19}$$

where λ_1 and λ_2 are Lagrange multipliers whose values are obtained by the satisfaction of the constraints (Equations (2.10) and (2.18)).

The procedure outlined above, along with specific choices for the stored energy function and the rate of dissipation, will now yield the appropriate rate-type model.

B. Convection-diffusion-reaction equations

The equations governing the flow and generation/depletion of the various constituents are all of the following form:

$$\frac{\partial [Y_i]}{\partial t} + div([Y_i]\mathbf{v}) = div(D_{Y_i}(\mathbf{D})\nabla[Y_i]) + G_{Y_i}; i = 1, ..., 25. \tag{2.20}$$

Here, and elsewhere below, $[Y_i]$ represents the concentration of the reactant Y_i, G_{Y_i} represents the production or depletion of Y_i due to the enzymatic reactions, $\mathbf{v}$ is the velocity field, and D_{Y_i} represents the diffusion coefficient of Y_i which could be a function of the shear rate (captured by means of the stretching tensor $\mathbf{D}$).

These constituents are assumed to co-exist at every point in the domain, and that, being of an extremely small composition, they do not affect the velocity of the bulk flow. The framework for studying the reaction-diffusion equations coupled with the flow equations is such that it allows a natural extension into a mixture theory model should the need arise.

C. Balance equations

The equations for the balance of mass, linear momentum, angular momentum, and internal energy are:

$$\frac{D\rho}{Dt} + \rho \mathrm{div}\mathbf{v} \;\; = \;\; 0\;, \tag{2.21}$$

$$\text{div}\mathbf{T} + \rho\mathbf{b} \;=\; \rho\frac{D\mathbf{v}}{Dt} \;, \tag{2.22}$$

$$\mathbf{T} \;=\; \mathbf{T}^{T} \;, \tag{2.23}$$

$$\rho\dot{\epsilon} \;=\; \mathbf{T}\cdot\mathbf{D} + \rho\Gamma - \text{div}\mathbf{q} \;. \tag{2.24}$$

Equation 2.23 is a statement of the balance of angular momentum in the absence of internal body forces. Here ρ is the density, $\mathbf{v}$ is the velocity field, $\mathbf{T}$ is the stress tensor, ϵ is the specific internal energy of the material, $\mathbf{D}$ is the stretching tensor, $\mathbf{q}$ is the heat flux, and Γ is the energy influx due to radiation.

CHAPTER III

BLOOD*

Blood exhibits non-Newtonian rheological behavior like shear-thinning properties and stress-relaxation behavior. A shear-thinning, viscoelastic fluid model with a deformation-dependent relaxation time is developed, and the efficacy of this model for describing the flow of human blood is tested. The model emerges in a hierarchy of nonsimple viscoelastic fluid models developed in a thermodynamic framework. The framework within which the model is developed leads to blood being characterised by four independent parameters that reflect the formation of rouleaux and its effect on the viscosity of blood, the shear thinning that takes place during the flow, the elasticity attributed to the RBC membrane, and the viscosity of the plasma. The model is corroborated with data from steady flow experiments (that report apparent viscosity) and oscillatory flow experiments. The model is then used to make predictions for the flow reversals when a pulsatile pressure gradient is applied to blood in a rigid-walled cylindrical tube, and also for the first normal stress differences, and these predictions are in keeping with physical expectations and match experimental data, respectively.

A.   Composition and rheological behavior

Whole blood consists of gel-like 'cell' matter in an aqueous plasma solution. The cell matter (which makes up around 46% of the volume in male human blood) consists of formed elements: primarily (around 98%) Red Blood Cells (RBCs) or erythrocytes, White Blood Cells (WBCs) or leukocytes, and platelets. The volume concentration of RBCs in whole blood is termed hematocrit. Plasma consists primarily in water

---

*Part of the material presented in this chapter is reprinted with permission from [5]. Copyright 2004 by International Journal of Cardiovascular Medicine and Science.

(92%-93%) in which various proteins (f-I or fibrinogen, f-II or prothrombin, f-V, f-VIII, f-IX, f-X, f-XI, f-XII, f-XIII, antithrombin-III, tissue-factor pathway inhibitor, protein C, protein S, plasminogen, α_1-antitrypsin, α_2-antiplasmin, etc.) are dissolved along with various ions (sodium (Na^+), potassium (K^+), calcium (Ca^{2+}), magnesium (Mg^{2+}), chloride (Cl^-), bicarbonate (HCO_3^-), phosphate (PO_4^{3-}), etc.). Plasma is a Newtonian liquid with a viscosity of approximately 1.2 cP [26]. Erythrocytes are biconcave deformable discs with no nuclei. The RBC membrane comprises 3% by weight of the entire RBC and consists of proteins (spectrin) and lipids. The RBC cytoplasm is a solution of hemoglobin in water (32g/100ml). Evans and Hochmuth [34] performed micropipette aspiration expirements which showed that RBCs display viscoelastic behavior. They also claimed that the viscoelastic nature of the RBC is only due to the viscoelastic properties of the RBC membrane. The leukocytes are classified as the granulocytes, the monocytes and the lymphocytes, and form less than 1% of the volume of blood. Their influence on the rheology of blood is not considered to be significant except in extremely small vessels like capillaries. Granulocytes exhibit viscoelastic properties [89] in micropipette aspiration experiments. Thus, the various constituents of blood exhibit different rheological properties.

The shear-thinning properties ([20],[26]) and stress-relaxation behavior ([96]) of whole blood are well known. The shear-thinning nature of blood has been tied to the disaggregation of the RBC-rouleaux aggregates that form at low shear (see Figure 3) and the deformability of the RBCs [24],[25], while its stress-relaxation properties are tied to the viscoelastic nature of the RBC membrane [34], [23] (see [101], [102] for a visualization of the microstructural changes that occur when blood is subject to oscillatory and steady shearing flow). The viscoelastic behavior of blood is less prominent at higher shear rates [97].
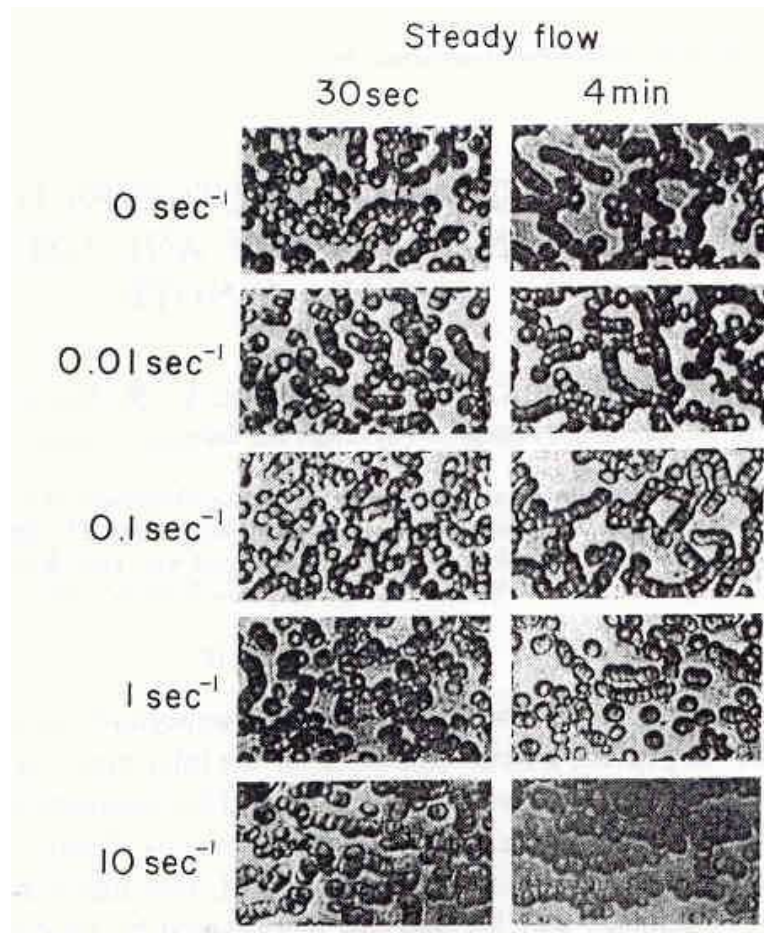
Fig. 3. Disaggregation of RBC-rouleaux aggregates upon application of steady shear flow. Reprinted from [112] with permission from IOS Press.

B. Literature survey of models

1. Continuum models

One of the early attempts to model blood as a continuum, with a yield stress, involved adapting the Casson's model for ink proposed in 1958 [19]. This model holds only for 1 dimensional flow situations, and can be used, at best, for fluid flow in axisymmetric rigid pipes. Continuum models have evolved, since then, to incorporate both the shear-thinning and viscoelastic behaviour of blood, and their dependence on the evolution of the underlying microstructure (the break-up and rearrangement of the rouleaux).

The Cross [30] and the Walburn and Schneck [116] models are among the earliest shear-thinning models, but can be used only in one-dimensional flow situations. A review of the various one-dimensional shear-thinning models with the myriad expressions for the apparent viscosity can be found in [27].

Phillips and Deutsch [77] proposed a four constant Oldroyd-B type of model that captured the rheological behavior of blood reasonably well. Thurston was among the earliest to attempt to incorporate the viscoelastic nature and the shear-thinning behavior of blood in a single model, and proposed an extended Maxwell model [100]. This model applies only in 1-D flow situations. Quemada [79] proposed a non-linear Maxwell model with an evolving internal variable (structural parameter) that underlies the change in viscosity with shear rate, and a similar generalization of the Maxwell model was proposed by Sharp and coworkers [91]. These models, like the ones proposed by Vlastos and coworkers [114], [115], are applicable only for one-dimensional flow situations.

Yeleswarapu [122] proposed a generalization of a three constant Oldroyd-B model that was an improvement over earlier three-dimensional viscoelastic models (see [122]

for a detailed literature survey of three-dimensional continuum models for blood flow), and captured the shear-thinning behavior of blood over very large shear rates.. Sun and De Kee [94] proposed a generalized Maxwell model for blood with an internal variable to capture the shear-thinning behavior. Their model has more parameters than the Yeleswarapu model and, like the Yeleswarapu model, has its limitations given that the relaxation times do not depend on the shear rate, a dependence that can be gleaned from experiments.

2. Dilute suspension, two-fluid, and mixture theory models

Kline and coworkers were among the earliest to propose that models of fluid suspensions be applied to blood flow. These models assume either that RBC deformations are negligible [53], or that RBC-RBC interactions and RBC-artery wall interactions are negligible [52], and do not have a sound physical basis in the light of what is currently known about RBC interactions during blood flow. Chaturani and coworkers proposed two fluid models for blood flow in small arteries [22], [21] based on the experimental observations of a erythrocyte rich core surrounded by a layer of plasma for flow in rigid walled small tubes. However, these models are valid only for small arterioles, and are not adequate for large arteries.

Trowbridge (1984) [105] proposed a model for blood as a binary mixture of erythrocytes and plasma. The model predicted a Newtonian behavior for the mixture and cannot, per se, be used to model blood.

C. A shear-thinning viscoelastic fluid model for blood

Whole blood is modeled as a shear-thinning viscoelastic fluid continuum with a deformation dependent relaxation time. The properties of this continuum are assumed

to depend on, and regulated by the various biochemical processes that take place and this is reflected in the basic balance laws for the continuum being coupled to and augmented by a system of convection-diffusion-reaction equations.

1.   Constitutive assumptions

The rate of dissipation ξ associated of the material is defined through

$$\xi = \mathbf{T} \cdot \mathbf{D} - \dot{W} \ . \tag{3.1}$$

The form chosen for the rate of dissipation in this study is

$$\xi = \alpha^b \left(\mathbf{D}_{\kappa_{\mathbf{p}(\mathbf{t})}} \cdot \mathbf{B}_{\kappa_{\mathbf{p}(\mathbf{t})}} \mathbf{D}_{\kappa_{\mathbf{p}(\mathbf{t})}} \right)^{\gamma^b} + \eta_1^b \mathbf{D} \cdot \mathbf{D}. \tag{3.2}$$

This form for the rate of dissipation corresponds to a mixture of a viscoelastic fluid that has a power-law viscosity (a generalized Maxwell fluid) and a Newtonian fluid. Such a choice is particularly appropriate as blood is a mixture of a Newtonian fluid (plasma) and the other constituents such as cells are elastic membranes containing fluids. The RBC-based microstructure evolves upon the application of shear, the evolution at a particular shear rate depending on the type of rouleau formed (at that shear rate), and becomes progressively liquid-like. While treating blood as a single continuum, we may thus include the entropy production due to the various mechanisms (viscous dissipation and disaggregation of rouleau structures). As a first step, it is assumed that these mechanisms are not interrelated. Additionally, it is assumed that the rate of dissipation is non-negative ($\alpha, \eta_1 > 0$) satisfying the second law.

The Helmholtz potential associated with the elastic response is assumed to be

that of a neo-Hookean material [1]:

$$W \equiv \rho\psi = \frac{\mu^b}{2}\left(I_{\mathbf{B}} - 3\right) . \tag{3.3}$$

Following the procedure of constrained maximisation outlined earlier, the following model is obtained (Equations (3.4)-(3.8)) [2]:

$$\mathbf{T} = -p\mathbf{1} + \mathbf{S} , \tag{3.4}$$

$$\mathbf{S} = \mu^b \mathbf{B}_{\kappa_{\mathbf{p}(\mathbf{t})}} + \eta_1^b \mathbf{D} , \tag{3.5}$$

$$\overset{\triangledown}{\mathbf{B}}_{\kappa_{p(t)}} = -2\left(\frac{\mu^b}{\alpha^b}\right)^{1+2n^b}\left(\mathrm{tr}(\mathbf{B}_{\kappa_{\mathbf{p}(\mathbf{t})}}) - 3\lambda\right)^{n^b}\left[\mathbf{B}_{\kappa_{p(t)}} - \lambda\mathbf{1}\right] , \tag{3.6}$$

$$\lambda = \frac{3}{\mathrm{tr}(\mathbf{B}^{-1}_{\kappa_{\mathbf{p}(\mathbf{t})}})} , \tag{3.7}$$

$$n^b = \frac{\gamma^b - 1}{1 - 2\gamma^b}; \quad n^b > 0. \tag{3.8}$$

The relaxation time governing the evolution of $\mathbf{B}_{\kappa_{\mathbf{p}(\mathbf{t})}}$ is $\left[2\left(\frac{\mu^b}{\alpha^b}\right)^{1+2n^b}\left(\mathrm{tr}(\mathbf{B}_{\kappa_{\mathbf{p}(\mathbf{t})}}) - 3\lambda\right)^{n^b}\right]^{-1}$, and is dependent on the elastic stretch. In like fashion, as the shear rate varies, the underlying rouleau size varies as does the corresponding relaxation time. However the relaxation time and the apparent viscosity (as seen from the equations that will be developed shortly) tend to ∞ as $\mathbf{D} \to \mathbf{0}$ (as shear rate tends to zero).

In order to ensure that the zero-shear viscosity is finite, a Heaviside function is introduced into the expressions for the viscosity and shear thinning index,

$$\alpha^b = \alpha_f^b \mathtt{H}(I_{\mathbf{B}} - I_0^b) + \alpha_0^b\left(1 - \mathtt{H}(I_{\mathbf{B}} - I_0^b)\right) , \tag{3.9}$$

---

[1]This choice corresponds to that for an isotropic material. However, directional effects may come into play due to the evolution of the rouleaux formations with the application of shear; a discussion of the issues underlying the choice of the Helmholtz potential can be found in [5].

[2]This model is not capable of an instantaneous elastic response. See discussion in [81].

$$\gamma^b \;=\; \gamma^b \mathtt{H}(\mathtt{I_B} - \mathtt{I}_0^b) + \left(1 - \mathtt{H}(\mathtt{I_B} - \mathtt{I}_0^b)\right), \tag{3.10}$$

$$\alpha_0^b \;=\; 2(\eta_0^b - \eta_\infty^b), \tag{3.11}$$

where η_0^b, η_∞^b are the asymptotic viscosities of blood at low and high shear rates, and $\mathtt{I}_0$ is a suitably chosen constant. The notation

$$\mathtt{K^b} = \left(\frac{\mu^b}{\alpha^b}\right)^{1+2n^b}, \tag{3.12}$$

is introduced for the sake of convenience.

D. Model corroboration

The parameters $\mathtt{K}^b, \mu^b, n^b$ and η_1^b, that are used in defining the model (Equations (3.4)-(3.8)) are determined so that the best fit is obtained for both steady flow data reporting apparent viscosity [122] and oscillatory flow data [98] of human blood [3]. The model is treated without reference to the detail in Equations (3.9)-(3.12). This is a minor detail, and can be fixed.

1. Apparent viscosity

Data for the apparent viscosity is reported from measurements in the rotating cylinder rheometer [122]. The material constants are inferred from measurements of torque and shear rate. Most commercial cylindrical rheometers (like the one used to obtain the data in [122]) employ a data reduction procedure based on a "small gap" assumption (see [118]). These approximate the shear rate at the wall by a constant mean value assuming that the variation of shear rate across the gap is small. The validity of such

---

[3]The model has also been used (with a different set of parameters) to match data for steady Poiseuille flow of porcine blood in rigid walled tubes [124], and the details can be found in [5]

an assumption is questionable for non-Newtonian liquids (see Yeleswarapu [122] for a brief parametric study of his model in such a flow situation). However, we proceed by assuming that the measured shear rate is a good approximation to the wall shear rate. It is preferable to use data (if available) reporting measured torques (or wall shear stresses) and angular speeds so that the intervening approximations may be reduced, and the material parameters may be fixed with greater precision. Data in the literature that has been reviewed is reported as apparent viscosity, though.

The flow field between the cylinders is assumed to be of the following form:

$$\mathbf{v} = u(r)\hat{\mathbf{e}}_\theta = rw(r)\hat{\mathbf{e}}_\theta \tag{3.13}$$

Substituting the constitutive equations (3.4)-(18) in the equations for balance of linear momentum and assuming an axisymmetric two dimensional stress field, the following expression is obtained for the wall shear stress (from which the torque is calculated):

$$T_{r\theta} = \left(\frac{\frac{\mu^b \lambda}{\chi} + \eta_1^b}{2}\right)\left(\frac{du}{dr} - \frac{u}{r}\right) . \tag{3.14}$$

Assuming that the shear rate is nearly constant across the gap ("thin gap assumption"), we obtain:

$$\frac{du}{dr} - \frac{u}{r} = R_\mathrm{O}\frac{\Delta w}{\delta r} , \tag{3.15}$$

where R_O is the radius of the outer cylinder, Δw is the difference in angular velocity between the outer and inner rotating cylinders, and δr represents the gap between the cylinders. The apparent viscosity reported for the model, given the torque and the shear rate, is:

$$\mu_{app} = \frac{\frac{\mu^b \lambda}{\chi} + \eta_1^b}{2} , \tag{3.16}$$

where λ is determined using the incompressibility condition: $\det(\mathbf{B}_{\kappa_{\mathbf{P(t)}}}) = 1$, and it

is given by:

$$\lambda = \frac{1}{\left[1 + \frac{1}{4\chi^2}(\frac{du}{dr} - \frac{u}{r})^2\right]^{1/3}} \ . \tag{3.17}$$

At any given shear rate, χ is obtained by solving:

$$\chi = \mathtt{K}^{\mathtt{b}}\left[\frac{2\dot{\gamma}_{meas}^2}{4\chi^2} \frac{1}{(1 + \frac{\dot{\gamma}_{meas}^2}{4\chi^2})^{1/3}}\right]^n \ , \tag{3.18}$$

where

$$\dot{\gamma}_{meas} = (\frac{du}{dr} - \frac{u}{r}) \ . \tag{3.19}$$

All four parameters are fixed using the expressions in Equations (3.16),(3.17),(3.18). For the limit $\dot{\gamma}_{meas} \to 0$, $\lambda \backslash \chi \to \infty$, but this can be fixed using Equations (3.9)-(3.12). For the limit $\dot{\gamma}_{meas} \to \infty$, $\lambda \backslash \chi = 0$ and $\eta_1 = 2\eta_\infty$. The multidimensional unconstrained minimisation procedure in MATLAB (fminsearch) is used to fix $\mathtt{K}$, μ and n for the best fit, with χ being solved by the fzero routine in MATLAB. The constants obtained (for human blood, $\eta_0^b = 0.0736 Pa.s$, $\eta_\infty^b = 0.005 Pa.s$) are $\mathtt{K}^b = 58.0725 s^{-1}$, $\mu^b = 0.1611 N/m^2$, $n^b = 0.5859$ (n must be positive to ensure shear-thinning behavior), and $\eta_1^b = 0.01 Pa.s$, and are but one among a very large selection that can fit the data equally well. The proposed model fits the experimental data better than the model proposed by Yeleswarapu at shear rates higher than 1 sec^{-1} (Figure 4).

2.   Application to oscillatory flow

The model parameters are fixed so that the amplitude of and phase difference between the pressure gradient and volume flow rate for oscillatory flow in a rigid-walled pipe obtained by numerical simulations matches the experimental data for a set of cases. This procedure is essential to validate the model over the gamut of flow conditions that are expected in the human vasculature. The set of experimental data that is used is just one among several sets of data available to infer the viscoelastic nature
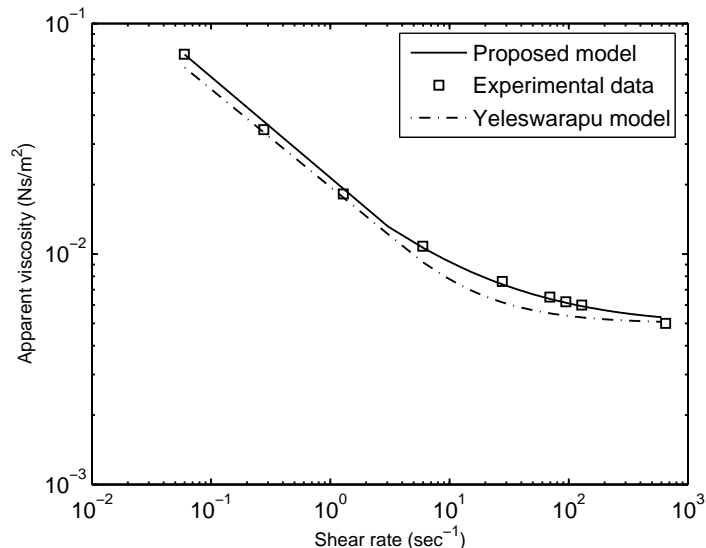
Fig. 4. Apparent viscosity of human blood. Predictions (of μ_{app}) from the proposed model, and the Yeleswarapu model are compared with the data [122].

of blood, and the model can be used to match these sets of data as well (for instance, the model can be used to match the stress-relaxation data in [68]).

Experimental data for the pressure gradient and volume flow (and the phase difference between them) under conditions of oscillatory and pulsatile flow through small tubes is available in [98] and [99]. The pressure gradient in phase with the volume flow rate (P'), and the component in quadrature with the volume flow rate (P'') are measured along with the (amplitude of) volume flow rate, and these are used to infer the values of the complex compliances (η',η''; see [117], [118] for an explanation of these quantities and a list of other experimental protocols by which they may be inferred). Such a data reduction procedure is not correct, given that we are dealing with a non-linear viscoelastic fluid; the pressure gradient and volume flow rate values from the numerical simulations are thus compared with the values of pressure gradient and volume flow rate reported in [98].

We seek a solution for oscillatory flow in a pipe of the form:

$$\mathbf{v} = u(r,t)\hat{\mathbf{e}}_z \ , \ p = p(r,z,t). \tag{3.20}$$

A time periodic solution is sought for $\mathbf{v}$, given the time periodicity of the imposed pressure gradient:

$$-\frac{1}{\rho^b}\frac{\partial p}{\partial z} = A\cos(wt) \ . \tag{3.21}$$

Upon substituting Equations (3.20),(3.21) into the balance of linear momentum, and assuming that the components of the stress depend only on the radial coordinate, the following equations are obtained (in non-dimensional form):

$$\frac{\partial u^*}{\partial t^*} = -\frac{\partial p^*}{\partial z^*} + \frac{S_{rz}^*}{r^*} + \frac{\partial S_{rz}^*}{\partial r^*} \ , \tag{3.22}$$

$$\frac{\partial B_{rz}}{\partial t^*} = \frac{\partial u^*}{\partial r^*}B_{rr} - 2\chi(\mathbf{B}_{\kappa_{p(t)}})\frac{R}{\mathsf{Ve}}B_{rz} \ , \tag{3.23}$$

$$\frac{\partial B_{rr}}{\partial t^*} = 2\chi(\mathbf{B}_{\kappa_{p(t)}})\frac{R}{\mathsf{Ve}}\left(\lambda - B_{rr}\right) \ , \tag{3.24}$$

$$\frac{\partial B_{zz}}{\partial t^*} = 2\frac{\partial u^*}{\partial r^*}B_{rz} + 2\chi(\mathbf{B}_{\kappa_{p(t)}})\frac{R}{\mathsf{Ve}}\left(\lambda - B_{zz}\right) \ , \tag{3.25}$$

where

$$S_{rz}^* = \frac{\mu^b}{\rho^b\mathsf{Ve}^2}B_{rz} + \frac{\eta_1^b}{2\rho^b R\mathsf{Ve}}\frac{\partial u^*}{\partial r^*} \ , \tag{3.26}$$

$$\lambda = \frac{3B_{rr}(B_{rr}B_{zz} - B_{rz}^2)}{B_{rr}^2 + 2B_{rr}B_{zz} - B_{rz}^2} \ , \tag{3.27}$$

$$\chi(\mathbf{B}_{\kappa_{p(t)}}) = \mathsf{K}^b\Big(2B_{rr} + B_{zz} - 3\lambda\Big)^{n^b} \ , \tag{3.28}$$

and R, Ve are the pipe radius and characteristic velocity respectively. (Note: $B_{\theta\theta} = B_{rr}$, $B_{r\theta} = B_{\theta z} = 0$).

The non-dimensionalisation is as follows: $t^* = t\mathsf{Ve}/R$, $w^* = wR/\mathsf{Ve}$, $u^* = u/\mathsf{Ve}$, $r^* = r/R$, $z^* = z/R$, $S_{rz}^* = S_{rz}/\rho\mathsf{Ve}^2$, $p^* = p/\rho\mathsf{Ve}^2$, and $A^* = AR/\mathsf{Ve}^2$.

The above PDEs are solved over the domain 0<r<1, for t≥ 0, subject to the

following boundary condition:

$$u^*(1, t) = 0 \ , \tag{3.29}$$

and center-line condition:

$$\frac{\partial u^*(0, t)}{\partial r^*} = 0 \ . \tag{3.30}$$

The exact solution for pulsatile flow of a Newtonian fluid [101] is set as the initial condition, whereas $\mathbf{B}_{\kappa_{\mathbf{p(t)}}} = \mathbf{1}$ is used as an initial guess for the components B_{rz}, B_{rr}, B_{zz}.

A predictor-corrector type numerical approach is used to solve the equations. The (coupled) PDEs are decoupled from each other, and the PDE for the velocity is treated as an IBVP, while the others are treated as IVPs. The coupling is brought about by means of an iterative process at each time step. The absence of the spatial derivative for B_{rz}, etc., (the components of $\mathbf{B}_{\kappa_{\mathbf{p(t)}}}$) in the appropriate equations, implies that it is enough to fix the boundary conditions for the velocity. Once the velocity is obtained, the values of the components of $\mathbf{B}_{\kappa_{\mathbf{p(t)}}}$ can be obtained over the entire domain (0≤r≤1).

The numerical simulations are performed ($\rho^b = 1053.6 kg/m^3$, Ve $= 1 cm/sec$) for a pipe of radius, R = 0.43 mm, at a frequency, f = 2Hz, in like manner to the experiments. The results of the simulation for a set of parameters that also fit the apparent viscosity data exceptionally well are given in Figure 5. The fit shown can be made better through better optimisation procedures, but such elaborate techniques are not adopted given the convergence characteristics of the numerical procedures.
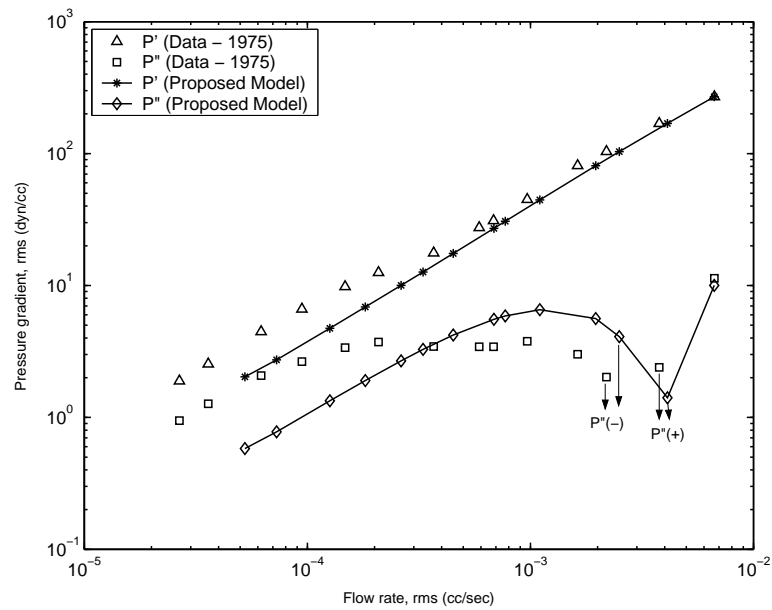
Fig. 5. Pressure (gradient) components in phase, P', and in quadrature, P'', with (amplitude of) volume flow rate for oscillatory flow of human blood in a rigid-walled pipe. The predictions of the proposed model ($K^b = 1.2056s^{-1}$, $\mu^b = 0.0227$ N/m^2, $n^b = 0.7525$, and $\eta_1^b = 0.01Pa.s$), are compared with data [98].

E.   Physical relevance of model predictions

The model predictions are obtained for flow in a rigid-walled pipe with a pulsatile pressure gradient of the form:

$$-\frac{1}{\rho}\frac{\partial p}{\partial z} = A(1 + cos(wt)) \ , \tag{3.31}$$

being applied.

The model predicts flow reversals, with the (relative) magnitude of flow reversal decreasing with increasing amplitude of the pressure gradient (Figure 6). This is a corroboration of the experimental evidence that the elastic properties of blood become less prominent with an increase in shear rate; inertial effects being more important at higher shear rates, and elastic effects dominating at low shear rates. It would be interesting to demonstrate this experimentally and to report the actual extent of flow reversal. However, no such data is available at the moment.

Copley and King [29] have reported measurements that show that blood manifests negligible normal stress differences during flow, and this observation is corroborated by the predictions of the first normal stress difference coefficient (ψ_1) by the model which (along with the predictions of the Yeleswarapu model) shows a steep drop in the normal stress difference at shear rates above 1 sec^{-1} (Figure 7). Precise numbers are not available, but, if such data is found, the model predictions for ψ_1 (ψ_1^M for the proposed model, and ψ_1^Y for the Yeleswarapu model) should be compared for quantitative accuracy.

$$\psi_1^M = \frac{(S_{zz} - S_{rr})}{\dot{\gamma}_{meas}^2} = \frac{\mu^b \lambda}{2\chi^2} \tag{3.32}$$

$$\psi_1^Y = \frac{(S_{zz} - S_{rr})}{\dot{\gamma}_{meas}^2} = 2\left(\nu(\dot{\gamma}_{meas})\lambda_1 - \eta_0\lambda_2\right) \tag{3.33}$$
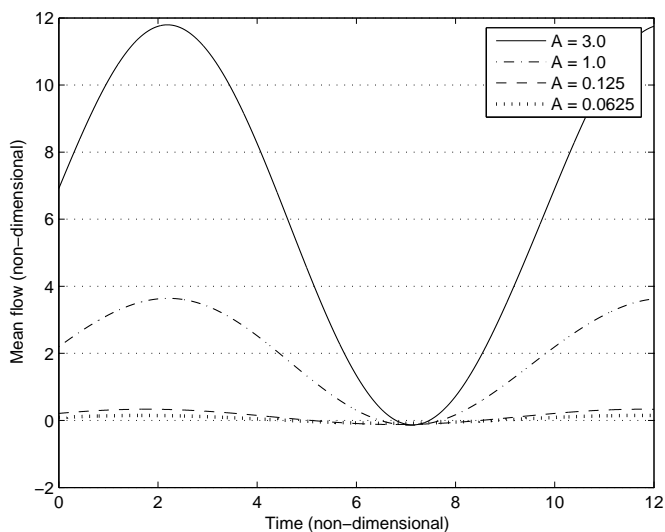
Fig. 6. Mean flow (and reversal) for various non-zero mean (Equation 3.31) pressure gradients predicted by proposed model
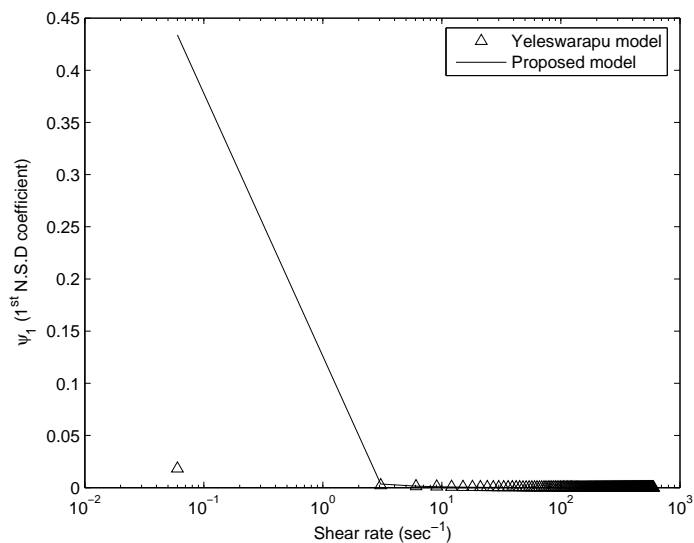
Fig. 7. First Normal stress difference for the flow of blood. The predictions of ψ_1 by the proposed model and the Yeleswarapu model are shown

CHAPTER IV

THE FORMATION AND DISSOLUTION OF CLOTS*

The formation and dissolution of clots in flowing blood is a complex phenomenon involving several biochemical and rheological changes that involve the components of blood, the flow regimes prevalent in the concerned region of the vasculature, and the surface of the vessel. A mathematical model consisting in a set of coupled convection-diffusion-reaction equations is developed to simulate the transport and biochemical changes of 25 consituents (present in human blood) that are essential to a complete, if not comprehensive, understanding of the phenomenon. The model (the reaction-diffusion equations) is corroborated with data for the formation and growth of a clot in quiescent platelet-poor plasma, and also with data for the dissolution of a formed clot in quiescent conditions. The entire set of equations is used to predict the consequences of Antithrombin-III (AT-III) deficiency and Protein-C (PC) deficiency, and the predictions match clinical data for the extreme severity of AT-III deficiency over PC deficiency.

A.   Biochemical and rheological changes accompanying hemostasis

Two important interacting processes, platelet activation followed by adhesion and aggregation, and coagulation, are initiated when there is an imbalance in favor of pro-thrombotic factors in flowing blood. This occurs in response to a variety of stimuli; an injury in the vessel wall, for instance, or contact with an exogenous foreign surface like glass, or imbalances between pro- and anti-thrombotic factors in the intact

endothelium itself ("Endothelial dysfunction" [40]), or due to certain flow conditions like stagnation and recirculation zones. The activated platelets that are generated can form aggregates by binding to each other and to fibrin, a stringy polymeric molecule formed at the end of the coagulation reactions. Coagulation involves a core cascade of enzymatic reactions [63], [31] involving plasma zymogens, anionic phoshpholipids on the membranes of activated platelets, and calcium ions resulting, ultimately, in the formation of thrombin from prothrombin, and then the cleavage of fibrinogen to yield fibrin. The platelet aggregates along with the fibrin mesh constitute the blood clot, and their formation comprises haemostasis, the normal response to vessel injury. Fibrin, along with other intermediates of the coagulation pathway and enzymes produced by endothelial cells, catalyze and participate in a set of reactions (fibrinolysis) that lead to the conversion of plasminogen to plasmin, thus initiating clot dissolution. This broad picture (see Figure 8) includes multiple positive and negative feedback loops and regulatory processes that involve the molecules in blood, its flow and the surface of the vessel (Virchow's triad). It is crucial that these processes act in a controlled fashion for the maintenance of vascular integrity without significant impairment to the flow of blood. A brief review of the main components and processes involved in the formation, development and dissolution of clots that will be incorporated in the model is given below; additional details and references can be found in [2].

1.   Platelet activation, adhesion and aggregation

Platelets form a small fraction (by volume) of the particulate matter in human blood (around 3%). They are among the most sensitive of all the components of blood to chemical and physical agents [58]. Platelets are small discoid cell fragments, approximately $6\mu m^3$ in volume, derived from megakaryocytes. Platelet activation is the

```
┌──────────────────────────┐
│   INJURY TO VESSEL WALL   │        ↕   INITIATION
│ /EXPOSURE TO −ve SURFACE  │            OF CLOTTIING
└──────────────────────────┘
```
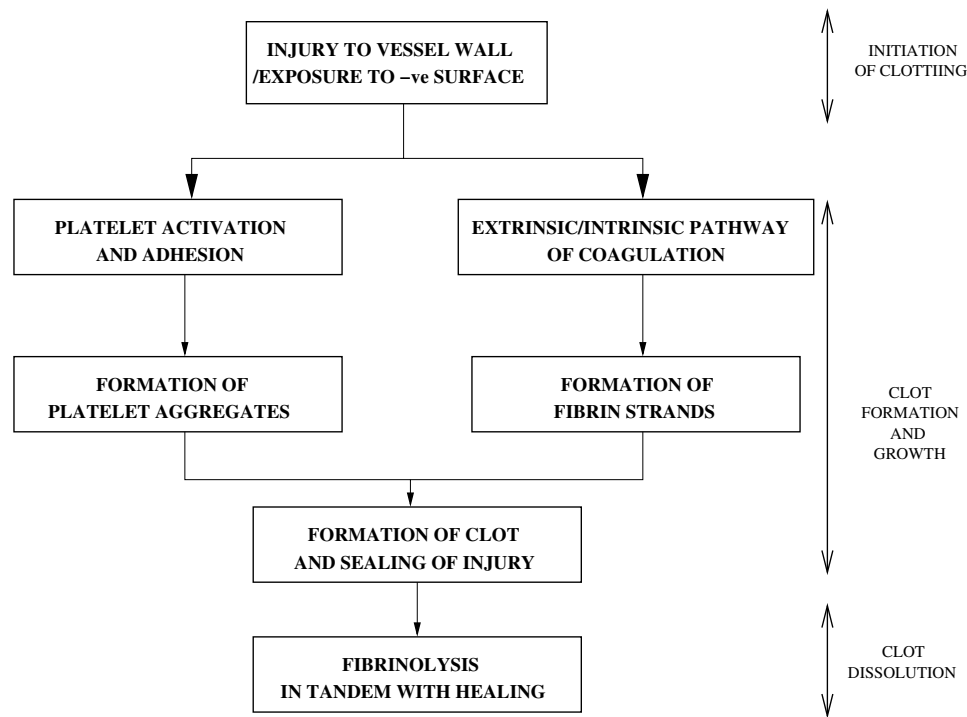
Fig. 8. An overview of the processes that occur during the formation and dissolution of clots.

process by which the resting discoid platelet undergoes a series of chemical and morphological changes as a result of which the organelles within the platelet are centralized, glycoproteins on the platelet membrane undergo a change in conformation, and long pseudopods are extended so that the activated platelet is a sticky spiny sphere. Platelet activation occurs due to interaction with collagens and adhesive glycoproteins exposed by rupture of the subendothelium, for instance, or due to interaction with thrombin or adenosine diphosphate (ADP) that circulate in the blood. Platelet activation is followed by interaction with plasma proteins like Factor-IX (IX), Factor-V (V), and vWF, fibrinogen, and fibrin so as to adhere to sub-endothelial tissue, form platelet aggregates, and ultimately form a clot. Activated platelets also release f-XIII, which through activation by thrombin, forms f-XIIIa that cross-links and stabilizes the fibrin matrix binding the clot. The rate and extent of platelet adhesion, platelet

deposition and platelet thrombus (or mural thrombus) formation are affected by the flow conditions (shear rates) [111]. Platelet activation itself [56], and sometimes lysis, is known to occur in response to prolonged exposure to high shear stresses [121]. Platelet aggregates, by themselves and as part of clots, are susceptible to break-up by high shear stresses [120], [85]. There are, thus, both biochemical changes and rheological influences during platelet activation, adhesion and aggregation.

2.   Extrinsic and Intrinsic pathways of coagulation

The extrinsic coagulation pathway is particularly important in the context of vessel wall injury. The exposure of tissue-factor (TF) (a cell membrane bound protein) in the subendothelium to the mainstream blood flow results in a chain of coagulation reactions (the extrinsic pathway) that lead to the formation of thrombin, an enzyme that catalyzes fibrin production and a very important enzyme for platelet activation. It is generally accepted that the formation of the TF-VIIa complex on the subendothelium leads to the formation of the enzymes, Factor-IXa (IXa) and Factor-Xa (Xa), both of which are serine proteases, from the respective plasma zymogens (enzyme antecedents), Factor-IX (IX) and Factor-X (X), after the cleavage of the prosequences. These enzymes, in turn, catalyze the formation of Factor-Va (Va) and Factor-VIIIa (VIIIa) from Factor-V (V) and Factor-VIII (VIII), respectively. The cascade of reactions that follows is the same (i.e., it involves the same species and the formation of the same intermediates), from here on, for both the extrinsic and intrinsic pathways, and is often referred to as the common pathway. The enzyme complex IXa-VIIIa bound to the membrane of the activated platelet (or negatively charged phospholipid, to be precise) catalyzes the formation of Xa from X. The membrane bound IXa-VIIIa complex is termed 'tenase'. The next important step in this chain is the formation of enzyme complex Xa-Va on the membrane of the activated platelet.

The membrane-bound Xa-Va complex ('prothrombinase') catalyzes the production of thrombin from prothrombin. Thrombin acts on fibrinogen (a plasma protein) to convert it to yield fibrin monomers that later polymerize and are cross-linked to form a fibrin matrix. The role of fibrinogen and fibrin in the coagulation reactions has been highlighted in a recent review [12].

The intrinsic coagulation pathway, is initiated when f-XII upon contact with a negatively charged surface (in this case, the collagen present in the subendothelial layer) is activated to XIIa by kallikrein. This activation is facilitated by high-molecular-weight-kininogen. XIIa activates the zymogen, f-XI, to its active enzyme form, XIa. XIa activates f-IX to IXa in the presence of Ca^{2+}. The reactions that follow are those of the common pathway, and lead to the formation of thrombin from prothrombin, and thence of fibrin from fibrinogen. The initiation of the intrinsic coagulation pathway by f-XII is relevant mainly in the in-vitro setting [37]. The intrinsic pathway is of great relevance for the laboratory monitoring of anticoagulation therapy for, and diagnosis of, coagulation disorders.

The biochemical changes during coagulation involve various positive and negative feedback loops within the broad framework outlined above. Thrombin and Xa play a major role in the positive feedback mechanisms by catalyzing the production of almost all the intermediates required for their production. Antithrombin-III (AT-III), Tissue factor pathway inhibitor (TFPI), and Active Protein C (APC) play a major role in inhibiting and regulating the coagulation cascade. The coagulation reactions and clot formation are known to be affected by mechanical factors like, for instance, the shear-rate dependence for the kinetics of fibrin formation. There are, thus, several biochemical changes during, and rheological influences on, the coagulation pathways.

3. Fibrinolysis

Fibrinolysis is initiated when thrombin and fibrin, formed during coagulation, activate endothelial cells resulting in enhanced production of tissue plasminogen activator (tPA) and urokinase-like plasminogen activator (uPA). tPA and uPA catalyze the transformation of plasminogen into the active enzyme plasmin. tPA is the more active among these two; its activity increases manifold in association with fibrin. Plasmin degrades the fibrin polymer into smaller units leading to the dissolution of the clot.

Like the coagulation pathways that precede it, fibrinolysis has its share of regulatory mechanisms. Active Protein C (APC), for example, is an accelarator of fibrinolysis. α_2-Antiplasmin (L2AP), and PAI-1, are plasma-phase enzymes that inhibit fibrinolysis by binding to fibrin. Clot dissolution can also occur due to mechanical factors like high shear stress, and the actual value depends on the composition of the clot. There are, thus, biochemical changes during, and rheological influences on, fibrinolysis and clot dissolution.

B. Literature survey of models

Mathematical models for the various stages of, and the several components involved in, clot formation and dissolution have expanded around the basic view (formulated in 1964) of the coagulation pathways (leading to thrombin production) as enzyme cascades [63], [31]. Levine proposed the earliest model (in 1966) for the enzyme cascade consisting in a set of first order ODEs [60]. Models later simulated the individual reactions of the coagulation pathway (like, for instance, the generation and depletion of prothrombinase [73]), and grew in compexity (in the late 1980s) to include the kinetics of sets of reactions in the enzyme cascade along with feedback

loops and inhibitors under different reaction conditions (like flow, extent of stimulus, etc.) [51], [48]. This trend continued so that models of greater complexity consisting in systems of coupled (linear or non-linear) ODEs [59], [57] and PDEs [126], [6] for platelet activitation, the coagulation pathways, and fibrinolysis [72], [32], were developed and have appeared in the literature in recent years (a detailed review of the literature can be found in [2]). As of the present, no single model has integrated all aspects of and changes during the formation and dissolution of clots in a single framework, and the model developed here is a step in this direction.

In the context of this historical trend, several important hypotheses emerged from the model simulations concerning the phenomenon of hemostasis. Among these, one of the most important is that of a threshold response of the coagulation pathways to the activating stimulus (whether, for the extrinsic pathway, the extent of injury, or, for the intrinsic pathway, the levels of f-XIa at the surface), and the observation that the threshold response is modulated by several factors (flow, the size of the injury, the availability of surface binding sites for the various constituents, the levels of Ca^{2+}, etc.); this hypothesis is observed primarily in the spatially homogeneous setting (the role of convection and diffusion is incorporated). Other hypotheses, observed in the context of the spatially inhomogeneous setting, are that the system for the coagulation pathways cannot return to its preactivation state without a steep drop in the activating stimulus itself, and the existence of a possible "effector" involved in the inhibition of clot growth [6]. An important hypothesis generated by the studies using PDEs to study the growth and elongation of clots in the spatially inhomogeneous setting is that, under quiescent conditions, the hemostatic mechanism, at least the coagulation pathways, are best characterized by reaction-diffusion equations in order to allow for stationary, spatially non-uniform solutions (as first described by Turing [108]) that mimic the structures that are formed during clot formation and growth.

Proceeding along this line of thought, a set of coupled convection-diffusion-reaction equations is postulated, and assumed to be best suited, to capture the influence of flow on, and the biochemical changes during, clot formation and dissolution in one single framework.

C. A model consisting in convection-diffusion-reaction equations for the various constituents

The formation, growth and dissolution of clots is modeled by means of a set of convection-diffusion-reaction equations that govern the transport and generation/depletion of the various enzymes, proteins and platelets that are involved. This set of equations is coupled to the balance laws of both blood and clot, and represents a unifying link with which to pull together the legs of Virchow's triad. Clot formation is initiated when an activation threshold in the flux boundary conditions is exceeded (related to the appearance of TF-VIIa complex on the injured surface, and the generation of XIa due to contact with the negatively charged collagen in the subendothelium; this is tied to the extent of the injury). The clot is said to be formed when the concentration of fibrin ([Ia]) equals or exceeds 600 nM. Clot growth is tied to the progress of the reactions, and is determined by tracking, in time, the extent of these regions. Fibrinolysis starts as soon as thrombin appears at the surface, and induces a rapid endothelial cell response. Clot dissolution occurs when fibrin ([Ia]) concentration drops below 600 nM or if the shear stress exceeds a critical value causing the clot to rupture.

The equations governing the movement and generation/depletion of the various constituents are of the following form:

$$\frac{\partial [Y_i]}{\partial t} + div([Y_i]\mathbf{v}) = div(D_{Y_i}(\mathbf{D})\nabla[Y_i]) + G_{Y_i}; i = 1, ..., 25. \qquad (4.1)$$

Here, and elsewhere below, $[Y_i]$ represents the concentration of the reactant Y_i, G_{Y_i} represents the production or depletion of Y_i due to the enzymatic reactions, $\mathbf{v}$ is the velocity, and D_{Y_i} represents the diffusion coefficient of Y_i which could be a function of the shear rate (captured by means of the stretching tensor $\mathbf{D}$).

The constituents are assumed to exist at every point in the domain, and that, being of an extremely small composition, they do not affect the velocity of the bulk flow. This framework of studying the reaction-diffusion equations coupled to the equations governing the flow of the continua (blood or clot) allows for a natural extension into a mixture theory model of interacting continua (involving all the components in blood).

The following constituents are assumed, among the several involved in clot formation and dissolution, to be of primary importance: resting platelets (RP), activated platelets (AP), fibrinogen & fibrin (I & Ia), prothrombin & thrombin (II & IIa), V & Va, VIII & VIIIa, IX & IXa, X & Xa, tenase (IXa-VIIIa-AP or 'Z'), prothrombinase (Xa-Va-AP or 'W'), XI & XIa, Antithrombin-III (ATIII), Protein C & Active protein C (PC & APC), Tissue factor pathway inhibitor (TFPI), α1-Antitrypsin (L1AT), Tissue Plasminogen Activator (tPA), Plasminogen (PLS) & Plasmin (PLA), and α2-Antiplasmin (L2AP). The role of the TF-VIIa complex, the generation of XIa at the surface due to contact activation, subendothelium-platelet interaction (the role of collagen and reactive proteins like vitronection, vWF, etc., in platelet activation, and the density of platelet binding sites), and endothelial cell tPA generation are included by means of flux boundary conditions. This list captures the broad aspects of clot formation but it is by no means comprehensive.

1.   Treatment of diffusion coefficients

The diffusion coefficients are tabulated in Table I; all the values are for platelets and proteins derived from human blood. The values, for platelets in human plasma at

37°C, are obtained using the Stokes-Einstein formula. The values, for the proteins, are obtained using a generalized form of the Stokes-Einstein equation (the correlation in [125]) that allows us to obtain the diffusion coefficients of the proteins in human plasma at 37°C.

Table I.: Diffusion coefficients

Species	Mol. Wt.	$\bar{\nu}$ (cc/g)	Diffusion coefficients (cm^2/sec)
RP	-	-	$D_{RP} = 1.58 \times 10^{-9}$
AP	-	-	$D_{AP} = 1.58 \times 10^{-9}$
I	340000	0.723	$D_I = 3.1 \times 10^{-7}$
Ia	$\approx$660000	0.730	$D_{Ia} = 2.47 \times 10^{-7}$
II	72000	0.719	$D_{II} = 5.21 \times 10^{-7}$
IIa	37000	0.730	$D_{IIa} = 6.47 \times 10^{-7}$
V	330000	0.730	$D_V = 3.12 \times 10^{-7}$
Va	179000	0.730	$D_{Va} = 3.82 \times 10^{-7}$
VIII	330000	0.730	$D_{VIII} = 3.12 \times 10^{-7}$
VIIIa	166000	0.730	$D_{VIIIa} = 3.92 \times 10^{-7}$
IX	56000	0.730	$D_{IX} = 5.63 \times 10^{-7}$
IXa	41000	0.730	$D_{IXa} = 6.25 \times 10^{-7}$
X	56000	0.730	$D_X = 5.63 \times 10^{-7}$
Xa	25000	0.730	$D_{Xa} = 7.37 \times 10^{-7}$
XI	160000	0.730	$D_{XI} = 3.97 \times 10^{-7}$
XIa	80000	0.730	$D_{XIa} = 5.0 \times 10^{-7}$
PC	62000	0.730	$D_{PC} = 5.44 \times 10^{-7}$
APC	60000	0.730	$D_{APC} = 5.50 \times 10^{-7}$

Table I.: (continued)

Species	Mol. Wt.	$\bar{\nu}$ (cc/g)	Diffusion coefficients (cm^2/sec)
ATIII	58000	0.730	$D_{ATIII} = 5.57 \times 10^{-7}$
TFPI	40000	0.730	$D_{TFPI} = 6.30 \times 10^{-7}$
L1AT	51000	0.728	$D_{L1AT} = 5.82 \times 10^{-7}$
tPA	68000	0.730	$D_{tPA} = 5.28 \times 10^{-7}$
PLS	92000	0.715	$D_{PLS} = 4.81 \times 10^{-7}$
PLA	85000	0.715	$D_{PLA} = 4.93 \times 10^{-7}$
L2AP	70000	0.720	$D_{L2AP} = 5.25 \times 10^{-7}$

2. Treatment of reaction kinetics

The reactions chosen to represent the extrinsic and intrinsic coagulation pathways, the generation of phospholipid binding sites due to platelet activation, the influence of thrombin on factor XIa generation, the formation of fibrin, and the generation of plasmin are given in the schematic (Figure 9). The reactions are listed in Table II, the form of the kinetics governing each constituent is detailed, and the kinetic constants are summarized in Table III. The reaction kinetic data is from available experiments; the enzyme kinetic data for all the reactions is for zymogens, enzymes, and platelets derived from human blood. Complete data for the kinetics governing the activation, and inactivation, of f-VIII, and f-VIIIa respectively, is not available. Given the large structural and functional similarities between f-V and f-VIII, the kinetic constants that govern the reactions involving f-VIII, and f-VIIIa, are assumed to be the same as those that govern the reactions involving f-V, and f-Va respectively. The kinetic data for the other zymogens and enzymes is taken from the relevant sources, and

details regarding the assumptions involved in choosing some of the constants can be found in a paper that is under preparation [3].

Some interactions, amidst the 25 constituents chosen, have not been included because of their relative insignificance like, for instance, the effect of Xa on V [69], and VIII [33], the effect of Xa on prothrombin (insignificant compared to the much faster reaction catalyzed by prothrombinase; see [55]), the effect of IXa on X [86], or the role of circulating TF [7]. The role of f-XII, not considered to be of major importance in the in-vivo setting [37], is included in the boundary conditions as a means of quantifying the generation of XIa at the surface.
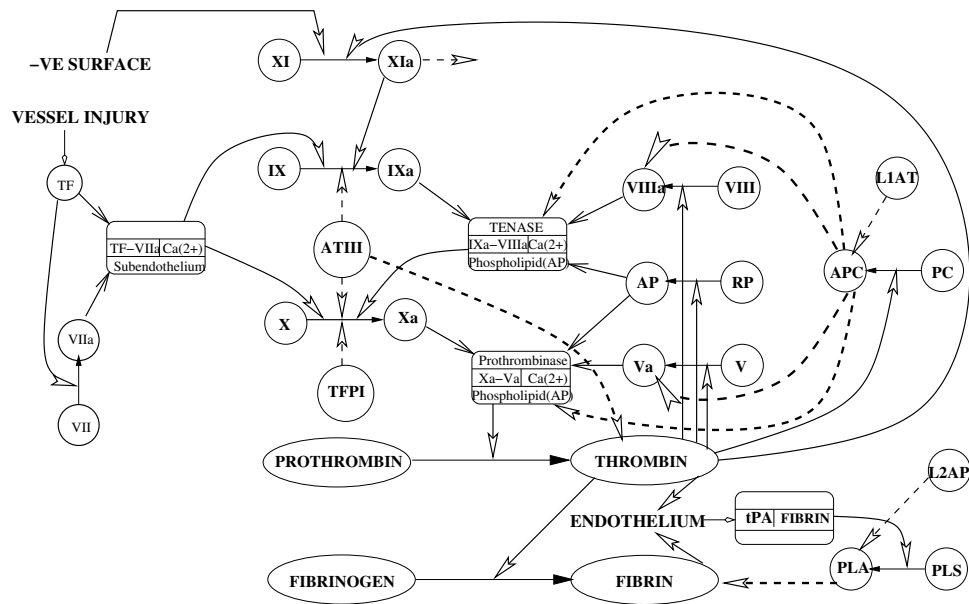
Fig. 9. Schematic of selected reactions involved in platelet activation, the extrinsic and intrinsic coagulation pathways and fibrinolysis. Solid lines denote zymogen activation or enzymatic catalysis. Broken lines denote enzymatic deactivation. Filled in arrow heads denote zymogen activation. Arrow heads that are not filled in denote enzymatic catalysis. Open arrow heads with solid lines denote participation in complex formation.

Table II.: Scheme of enzymatic reactions.

$(Z = \text{IXa-VIIIa-AP} , W = \text{Xa-Va-AP})$

	Activation			Inactivation	
(1a)	k_{11},K_{11m}	XI $\xrightarrow{\text{IIa}}$ XIa	(1b)	h_{11}^{A3}	XIa + ATIII $\rightarrow$ XIa-ATIII
			(1c)	h_{11}^{L1}	XIa + L1AT $\rightarrow$ XIa-L1AT
(2a)	k_9,K_{9M}	IX $\xrightarrow{\text{XIa}}$ IXa	(2b)	h_9	IXa + ATIII $\rightarrow$ IX$_i$
(3a)	k_8,K_{8M}	VIII $\xrightarrow{\text{IIa}}$ VIIIa	(3b)	h_8	VIIIa $\rightarrow$ VIII$_i$
			(3c)	h_{C8}	VIIIa $\xrightarrow{APC}$ VIII$_i$
(4a)	K_{dZ}	VIIIa + IXa $\xrightarrow{\text{AP}}$ Z Z $\xrightarrow{\text{AP}}$ VIIIa + IXa			
(5a)	k_5,K_{5M}	V $\xrightarrow{\text{IIa}}$ Va	(5b)	h_5	Va $\rightarrow$ V$_i$
			(5c)	h_{C5},H_{C5M}	Va $\xrightarrow{APC}$ V$_i$
(6a)	k_{10},K_{10M}	X $\xrightarrow{Z}$ Xa	(6b)	h_{10}	Xa + ATIII$\rightarrow$ Xa-ATIII
			(6c)	h_{TFPI}	Xa + TFPI$\rightarrow$ Xa-TFPI
(7a)	K_{dW}	Va + Xa $\xrightarrow{\text{AP}}$ W W $\xrightarrow{\text{AP}}$ Va + Xa			
(8a)	k_2,K_{2m}	II $\xrightarrow{W}$ IIa	(8b)	h_2	IIa + ATIII$\rightarrow$ IIa-ATIII
(9a)	k_{PC},K_{PCM}	PC $\xrightarrow{\text{IIa}}$ APC	(9b)	h_{PC}	APC + L1AT$\rightarrow$APC-L1AT
(10a)	k_1,K_{1m}	I $\xrightarrow{\text{IIa}}$ Ia	(10b)	h_1,H_{1m}	Ia + PLA $\rightarrow$ I$_i$
(11a)	k_{AP}^{IIa}	RP $\xrightarrow{\text{IIa}}$ AP			
(11b)	k_{AP}^{AP}	RP $\xrightarrow{\text{AP}}$ AP			
(12a)	k_{PLA}^{tPA-Ia} K_{PLAm}	PLS$\xrightarrow{tPA-Ia}$PLA	(12b)	h_{PLA}	PLA + L2AP$\rightarrow$PLA-L2AP

The rate of depletion of a zymogen is equal to the rate of its activation into the

corresponding enzyme. The corresponding enzyme is generated from the zymogen and is depleted by inactivation due to inhibitors. The generation and depletion of the 25 constituents is described by the following ordinary differential equations:

$$\frac{d[XIa]}{dt} = \frac{k_{11}[IIa][XI]}{K_{11M} + [XI]} - h_{11}^{A3}[XIa][ATIII] - h_{11}^{L1}[XIa][L1AT] = G_{XIa} \quad (4.2)$$

$$\frac{d[XI]}{dt} = -\frac{k_{11}[IIa][XI]}{K_{11M} + [XI]} = G_{XI} , \quad (4.3)$$

$$\frac{d[IXa]}{dt} = \frac{k_9[XIa][IX]}{K_{9M} + [IX]} - h_9[IXa][ATIII] = G_{IXa} , \quad (4.4)$$

$$\frac{d[IX]}{dt} = -\frac{k_9[XIa][IX]}{K_{9M} + [IX]} = G_{IX} , \quad (4.5)$$

$$\left[Z\right] = \frac{[VIIIa][IXa]}{K_{dZ}} , \quad (4.6)$$

$$\frac{d[Xa]}{dt} = \frac{k_{10}[Z][X]}{K_{10M} + [X]} - h_{10}[Xa][ATIII] - h_{TFPI}[TFPI][Xa] = G_{Xa} , \quad (4.7)$$

$$\frac{d[X]}{dt} = -\frac{k_{10}[Z][X]}{K_{10M} + [X]} = G_X , \quad (4.8)$$

$$\left[W\right] = \frac{[Va][Xa]}{K_{dW}} , \quad (4.9)$$

$$\frac{d[AP]}{dt} = k_{AP}^{AP}[AP][RP] + k_{AP}^{IIa}[RP] = G_{AP}, \quad (4.10)$$

$$\frac{d[RP]}{dt} = -G_{AP} = G_{RP} , \quad (4.11)$$

$$\frac{d[IIa]}{dt} = \frac{k_2[W][II]}{K_{2M} + [II]} - h_2[IIa][ATIII] = G_{IIa} , \quad (4.12)$$

$$\frac{d[II]}{dt} = -\frac{k_2[W][II]}{K_{2M} + [II]} = G_{II} , \quad (4.13)$$

$$\frac{d[VIIIa]}{dt} = \frac{k_8[IIa][VIII]}{K_{8M} + [VIII]} - h_8[VIIIa] - h_{C8}[APC] = G_{VIIIa} , \quad (4.14)$$

$$\frac{d[VIII]}{dt} = -\frac{k_8[IIa][VIII]}{K_{8M} + [VIII]} = G_{VIII} , \quad (4.15)$$

$$\frac{d[Va]}{dt} = \frac{k_5[IIa][V]}{K_{5M} + [V]} - h_5[Va] - \frac{h_{C5}[APC][Va]}{H_{C5M} + [Va]} = G_{Va} , \quad (4.16)$$

$$\frac{d[V]}{dt} = -\frac{k_5[IIa][V]}{K_{5M} + [V]} = G_V , \quad (4.17)$$

$$\frac{d[APC]}{dt} = \frac{k_{PC}[IIa][PC]}{K_{PCM} + [PC]} - h_{PC}[APC][L1AT] = G_{APC} , \quad (4.18)$$

$$\frac{d[PC]}{dt} = -\frac{k_{PC}[IIa][PC]}{K_{PCM} + [PC]} = G_{PC} \, , \tag{4.19}$$

$$\frac{d[ATIII]}{dt} = -(h_9[IXa] + h_{10}[Xa] + h_2[IIa] + h_{11}^{A3}[XIa])[ATIII] = G_{[ATIII]}, \tag{4.20}$$

$$\frac{d[TFPI]}{dt} = -h_{TFPI}[TFPI][Xa] = G_{TFPI} \, , \tag{4.21}$$

$$\frac{d[L1AT]}{dt} = -h_{PC}[APC][L1AT] - h_{11}^{L1}[XIa][L1AT] = G_{L1AT} \, , \tag{4.22}$$

$$\frac{d[Ia]}{dt} = \frac{k_1[IIa][I]}{K_{1M} + [I]} - \frac{h_1[PLA][Ia]}{H_{1M} + [Ia]} = G_{Ia}, \tag{4.23}$$

$$\frac{d[I]}{dt} = -\frac{k_1[IIa][I]}{K_{1M} + [I]} = G_I, \tag{4.24}$$

$$\frac{d[tPA]}{dt} = 0 = G_{tPA} \, , \tag{4.25}$$

$$\frac{d[PLA]}{dt} = k_{PLA}^{tPA-Ia}[tPA] - h_{PLA}[PLA][L2AP] = G_{PLA} \, , \tag{4.26}$$

$$\frac{d[PLS]}{dt} = -k_{PLA}^{tPA-Ia}[tPA] = G_{PLS} \, , \tag{4.27}$$

$$\frac{d[L2AP]}{dt} = -h_{PLA}[PLA][L2AP] = G_{L2AP} \, . \tag{4.28}$$

Table III.: Reaction rates and kinetic constants. The following notation is used: M = Michaelis-Menten kinetics, F = First order kinetics, S = Second order kinetics.

Reaction	Kinetics	Parameters	Sources
(1a)	M	$k_{11} = 0.0078\ min^{-1}$, $K_{11M} = 50$ nM	[38]
(1b)	S	$h_{11}^{A3} = 3\times10^{-5}\ nM^{-1}min^{-1}$	[90]
(1c)	S	$h_{11}^{L1} = 1.3\times10^{-5}\ nM^{-1}min^{-1}$	[90]
(2a)	M	$k_9 = 11\ min^{-1}$, $K_{9M} = 160$ nM	[95]
(2b)	S	$h_9 = 0.0162\ nM^{-1}min^{-1}$	[119]
(3a)	M	$k_8 = 27.0\ min^{-1}$, $K_{8M} = 140.5$ nM	see text
(3b)	F	$h_8 = 0.222\ min^{-1}$	[74]
(3c)	M	$h_{C8} = 10.2\ min^{-1}$, $H_{C8M} = 14.6$ nM	see text
(4a)	S	$K_{dZ} = 0.56\ nM$	[1]
(5a)	M	$k_5 = 27.0\ min^{-1}$, $K_{5M} = 140.5$ nM	[69]
(5b)	F	$h_5 = 0.17\ min^{-1}$	[36]
(5c)	M	$h_{C5} = 10.2\ min^{-1}$, $H_{C5M} = 14.6$ nM	[92]
(6a)	M	$k_{10} = 2391\ min^{-1}$, $K_{10M} = 160$ nM	[83]
(6b)	S	$h_{10} = 0.347\ nM^{-1}min^{-1}$	[119]
(6c)	S	$h_{TFPI} = 0.96\ nM^{-1}min^{-1}$	[57]
(7a)	S	$K_{dW} = 0.1\ nM$	[65]
(8a)	M	$k_2 = 1344\ min^{-1}$, $K_{2m} = 1060\ nM$	[55]
(8b)	S	$h_2 = 0.714\ nM^{-1}min^{-1}$	[119]
(9a)	M	$k_{PC} = 39\ min^{-1}$, $K_{PCM} = 3190$ nM	[107]
(9b)	S	$h_{PC} = 6.6\times10^{-7}\ nM^{-1}min^{-1}$	[45]

Table III.: (continued)

Reaction	Kinetics	Parameters	Sources
(10a)	M	$k_1 = 3540\ min^{-1}$, $K_{1m} = 3160\ nM$	[107]
(10b)	M	$h_1 = 1500\ min^{-1}$, $H_{1m} = 250000\ nM$	[32]
(11a)	F	$k_{AP}^{IIa} = 22.2\ min^{-1}$	[57]
(11b)	S	$k_{AP}^{AP} = 18\ nM^{-1}min^{-1}$	[57]
(12a)	M	$k_{PLA}^{tPA-Ia} = 12\ min^{-1}$, $K_{PLAm} = 18nM$	[64]
(12b)	S	$k_{L2AP} = 0.096\ nM^{-1}min^{-1}$	[54]

D. Model corroboration

The model equations are corroborated by comparing the results of simulations with the experimental data for clot formation and elongation in quiescent plasma on a monolayer of (tissue-factor generating) fibroblasts, and for the dissolution of (formed) clots in quiescent plasma.

1. Clot formation and growth in quiescent plasma

The formation and growth of a clot is documented in quiescent platelet poor plasma (normal human, hemophiliac : A/B) for various surfaces (glass, PTFE, monolayers of human fibroblasts[76], aortic endothelial cells [75]). The clot growth is followed by measuring the intensity of scattered light, and the spatio-temporal dynamics of the phenomenon is thus recorded. The light-scattering intensity is correlated to the fibrin concentration. The data for the clot growth on a monolayer of (tissue-factor generating) human fibroblasts [76] is used, the experimental conditions are matched in the simulations, and the numerical results are matched with the experimentally

recorded curves for clot growth. In simulating the data, it is assumed that the clot grows uniformly over the activating surface, so that only one spatial dimension (the domain is of length 'L', and the coordinate 'x' varies from 0 to L) and time are important.

The reaction-diffusion equations (convection is not present in this case) corresponding to the 25 constituents are used, the initial conditions are set to be the physiologic concentrations of the constituents in human plasma (Table IV), and the boundary conditions (see below) are picked to account for the simultaneous stimulation of the extrinsic and intrinsic pathways (fibrinolysis is not relevant for this case, and the boundary conditions are set to account for this fact). The equations are solved using the 'pdepe' routine available in MATLAB.

Table IV.: Initial concentrations for some of the constituents involved in clot formation and dissolution.

Species	Initial concentration (nM)	Reference
RP	10	[57]
AP	0.5	[93]
I	7000	[66]
Ia	0	
II	1400	[66]
IIa	0	
V	20	[66]
Va	0	
VIII	0.7	[66]
VIIIa	0	

Table IV.: (continued)

Species	Initial concentration (nM)	Reference
IX	90	[66]
IXa	0	
X	170	[66]
Xa	0	
XI	30	[15]
XIa	0	
ATIII	2410	[10]
TFPI	2.5	[66]
PC	60	[66]
APC	0	
L1AT	45000	[28]
tPA	0.08	[14]
PLS	2180	[61]
PLA	0	
L2AP	105	[28]

The concentration boundary condition at the end of the domain (x = L) is

$$\frac{\partial [Y_i]}{\partial x}\bigg|_{x=L} = 0 \ , \tag{4.29}$$

for all constituents 'Y_i' (i.e., i = 1,...,25). This condition ensures that this end of the domain is impermeable to the boundary flux of all the constituents.

The concentration boundary conditions at the surface (x = 0) are

$$\frac{\partial[Y_i]}{\partial x}\Big|_{x=0} = 0 \ , \tag{4.30}$$

for all constituents 'Y_i' except XIa, XI, IXa, IX, Xa, X, AP, RP, and tPA.

The boundary conditions at the wall for these nine species are as follows:

$$\frac{\partial[XIa]}{\partial x}\Big|_{x=0} = \frac{\phi_{11}[XIIa][XI]}{\Phi_{11M} + [XI]}\frac{L}{D_{XIa}} = -\frac{D_{XI}}{D_{XIa}}\frac{\partial[XI]}{\partial x}\Big|_{x=0} \ , \tag{4.31}$$

$$\frac{\partial[IXa]}{\partial x}\Big|_{x=0} = \frac{k_{7,9}[IX][TF-VIIa]}{K_{7,9M} + [IX]}\frac{L}{D_{IXa}} = -\frac{D_{IX}}{D_{IXa}}\frac{\partial[IX]}{\partial x}\Big|_{x=0} \ , \tag{4.32}$$

$$\frac{\partial[Xa]}{\partial x}\Big|_{x=0} = \frac{k_{7,10}[X][TF-VIIa]}{K_{7,10M} + [X]}\frac{L}{D_{Xa}} = -\frac{D_{X}}{D_{Xa}}\frac{\partial[X]}{\partial x}\Big|_{x=0} \ , \tag{4.33}$$

$$\frac{\partial[AP]}{\partial x}\Big|_{x=0} = k_{AP}[SUBENDO][RP]\Big|_{x=0}\frac{L}{D_{AP}} = -\frac{D_{RP}}{D_{AP}}\frac{\partial[RP]}{\partial x}\Big|_{x=0} \ , \tag{4.34}$$

$$\frac{\partial[tPA]}{\partial x}\Big|_{x=0} = (k_{tPA}^{C} + k_{tPA}^{IIa}[IIa]\Big|_{x=0} + k_{tPA}^{Ia}[Ia]\Big|_{x=0})[ENDO]\frac{L}{D_{tPA}} \ . \tag{4.35}$$

The details pertaining to the model corroboration (the reduction of the experimental data to fibrin concentration curves, the details concerning the numerical implementation and the kinetic parameters governing the boundary conditions), and the final results matching the model-generated curves and data, are the subject matter of a paper that is under preparation [3].

2. Clot dissolution in quiescent plasma

The dissolution of a clot formed from platelet poor plasma, and subject to the action of tPA introduced into the quiescent plasma surrounding the clot, is recorded [87]. Clot lysis is followed by means of confocal fluorescence microscopy, and the rate of clot lysis is estimated from these images (Figure 10). The data for the clot extent in time is used, the experimental conditions are matched in the simulations, and the numerical results are matched with the experimental data. In simulating the data, it

is assumed that clot dissolution occurs uniformly, and proceeds radially inward with time (only one spatial dimension, and time are considered).

The reaction-diffusion equations corresponding to 5 constituents (Ia, tPA, PLS, PLA, L2AP) are used, the initial conditions are picked appropriately given that there are two distinct regions (the circular clot region, and the platelet-poor plasma region surrounding it), and the boundaries of the domain are set to be impermeable. The equations are solved using the 'pdepe' routine in MATLAB.

The details pertaining to the model corroboration (the reduction of the experimental data to the clot extent region, the details of the numerical implementation) are the subject matter of a paper that is under preparation [3], and the final results will be presented in that paper.

E.   Clinical correlations of model predictions

The predictions of the model are obtained for the case of clot formation and dissolution in quiescent (Antithrombin-III deficient and Protein C deficient)plasma on a thrombogenic surface in-vitro. Only one spatial dimension and time are considered, and the dynamics of the process are investigated in a 2 mm domain over a time interval of 3600 seconds. The entire set of model equations is studied, with the appropriate initial conditions (Table IV), and boundary conditions picked to account for a simultaneous activation of the extrinsic and intrinsic pathways, and for the fibrinolytic pathway. The equations are solved using the 'pdepe' routine in MATLAB.

The predictions of the time for initiation of clot formation (Figure 11), the maximum size reached by the clot before dissolution (Figure 12), and the maximum concentration of fibrin reached within the clot (tied to the fracture strength of the clot) during growth (Figure 13) are obtained for varying levels of Antithrombin-III

and Protein-C deficiency. The initiation times for clotting become very small as AT-III deficiency reaches 40%, suggesting severe thrombotic complications at such levels. The results, in general, suggest that AT-III deficiency has far more profound consequences on all these parameters, and thus severe clinical implications, than does Protein-C deficiency, and this is fully in keeping with clinical data for these hypercoagulable states [17], [67]. These results, and their relevance for clinical practice, will be discussed in complete detail in the paper that is under preparation [3].
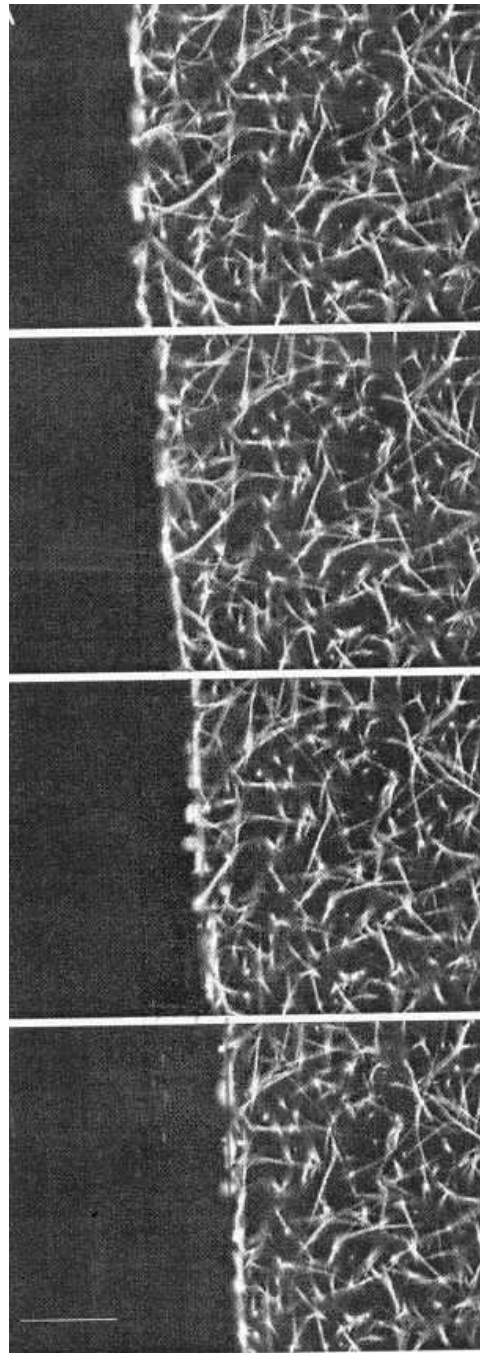
Fig. 10. Clot lysis: Rearrangements of the fibrin network of a plasma clot during lysis induced by t-PA present in plasma surrounding the clot. The four consecutive images were made 20 minutes after the addition of t-PA with 30-s intervals between the images. Reprinted from [87] with (automatic) permission from ASBMB.
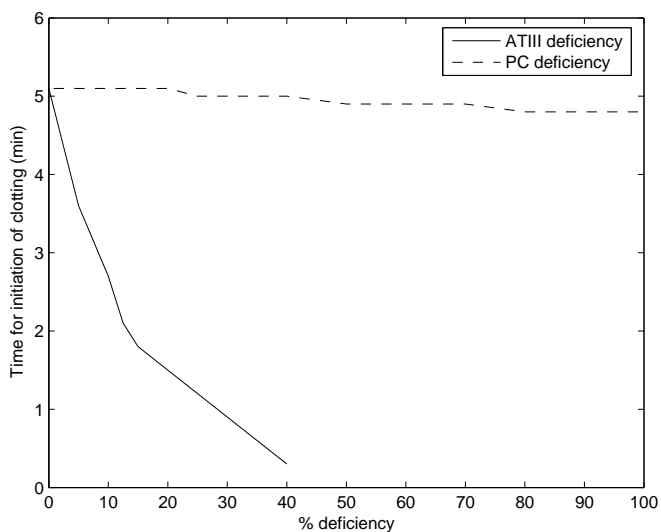
Fig. 11. Model predictions of the time for initiation of clot formation, for varying levels of Antithrombin-III and Protein-C deficiency.
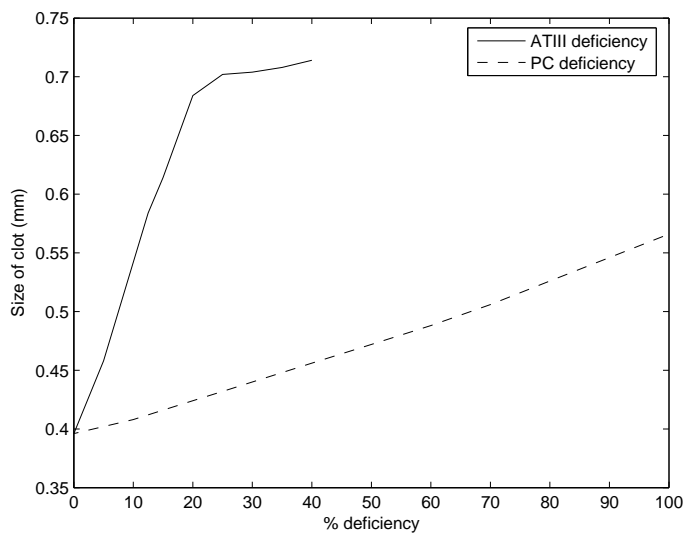
Fig. 12. Model predictions of the maximum size reached by the clot before dissolution, for varying levels of Antithrombin-III and Protein-C deficiency.
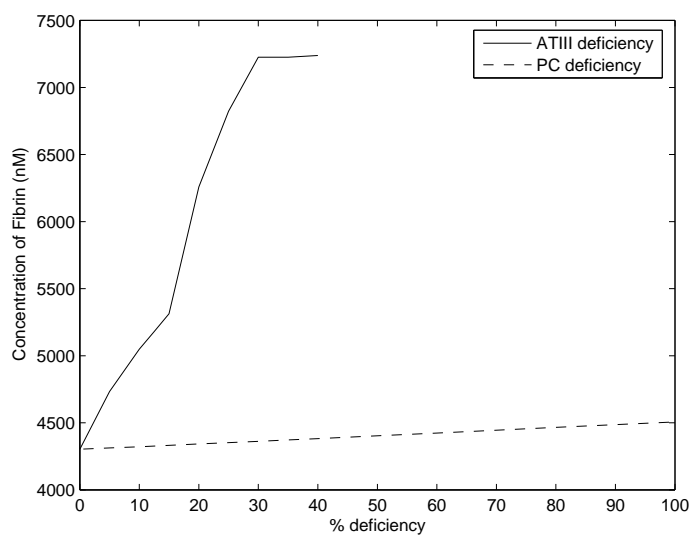
Fig. 13. Model predictions of the maximum concentration of fibrin reached within the clot during growth, for varying levels of Antithrombin-III and Protein-C deficiency.

CHAPTER V

CLOTS[*]

 A clot consists of a fibrin matrix bound to platelet aggregates within which RBCs, WBCs, and plasma are entrapped. The fibrin fibers typically form a very small part of the entire structure (less than 1% by volume; see [13]). Clots exhibit viscoelastic behavior, and this viscoelastic behavior varies dramatically based on the architecture of the underlying fibrin matrix (see [35]). The time scales over which the clot is considered a viscoelastic liquid vary significantly based on the fibrin matrix architecture. A viscoelastic fluid model is developed, and the efficacy of this model in describing the flow of an intravascular thrombus is tested. The framework within which the model is developed leads to the clot being characterized by four parameters that govern the dissipation due to the deformation of the fibrin matrix and the platelets, RBCs, WBCs and plasma bound to this matrix, the energy stored during the deformation of the fibrin matrix, and the dissipation due to the motion of the plasma itself. The model is corroborated with data for oscillatory flow in a small diameter rigid-walled pipe. The model is then used to make predictions for the apparent viscosity that would be inferred in steady flow experiments, and the predictions are in keeping with physical expectations.

A.   Composition and rheological behavior of various types of clots

There are three types of clots: fibrin clots, plasma clots and whole blood clots. Fibrin clots are formed from fibrinogen solutions treated with thrombin. Plasma clots are formed from plasma after treatment with thrombin and calcium chloride (added to

---

[*]Part of the material presented in this chapter will appear in an article that has been accepted for publication [4].

enhance platelet activation). Whole blood clots are formed in-vitro from (usually citrated) blood by addition of calcium chloride. In all these clots the fibrin matrix is formed due to the same basic set of reactions: the polymerization of fibrin monomers after fibrinogen is acted upon by thrombin, and the cross-linking of the fibrin strands by the action of XIIIa. *Ligated* clots are clots where the fibrin fibers are crosslinked (through the action of XIIIa), whereas *unligated* clots are those where the fibrin structure does not have these crosslinks. Clots are also classified based on the pH and ionic strength during formation: 1. *fine* fibrin clots are formed at relatively high pH (around 8.0 and above) and ionic strength (around 0.45M), 2. *coarse* fibrin clots are formed at lower pH (around 7.4-7.5) and ionic strength (around 0.15M), or in conditions that are close to physiological conditions. Coarse fibrin clots are characterized by extensive lateral aggregation of fibrin strands, the typical diameter of the fibrin strand bundle being greater than 200 $\overset{o}{A}$. Fine fibrin clots do not have such extensive lateral aggregation and consist of single strands of the fibrin polymer, the typical diameter of the fibrin strand being around 10 $\overset{o}{A}$. Turbidity measurement is one of the methods used to detect the diameter of the fibrin strands and the strand bundles (see [18]).

The creep data for coarse ligated and coarse unligated fibrin clots formed from human fibrinogen suggest a viscoelastic liquid-like response over time scales of $\sim$3500 sec and 2500 sec, respectively ([39]). Creep data for fine ligated and fine unligated fibrin clots formed from human fibrinogen (pH = 8.5, aged for 6 and 7 hours respectively) suggest a viscoelastic liquid-like response over time scales of $\sim$14000 sec and 10000 sec, respectively ([70], [71]). Stress relaxation data for a fine unligated fibrin clot (ph = 8.5, aged for 20 hours) confirm that the time scale over which it may be considered a viscoelastic liquid is around 10000 sec ([47]). In general, clot properties are very sensitive to the concentration of fibrinogen and platelets (see [41],

[42]), hematocrit (volume concentration of RBCs) of blood sample (see [84]), ionic strength (concentration of $NaCl$ and phosphates) and Ca^{2+} concentration (see [35]), the flow conditions (shear rate etc.) during clot formation (see [84]), and the age of the clot. However, complete data on all these parameters are often not found, or when given, do not match exactly. The above estimates for the time scales of viscoelastic liquid-like response are for clots formed under very similar conditions, and aged for comparable lengths of time.

There are many experimental methods used to record the viscoelastic properties of clots; notable among these are studies that employ the Weissenberg rheogoniometer ([42]), the Thromboelastograph ([44]), the damped oscillation type rheometer (a list of references can be found in the review article by Kaibara [49]), and the capillary viscometer ([104]). Studies characterizing the viscoelastic behavior of clots tend to report data in terms of linear viscoelastic parameters (G' and G", see [78] for an explanation of these terms). Such data is of little value while corroborating nonlinear 3D models. The stress relaxation (data reporting stress versus time at fixed strain) and creep data (data reporting strain versus time at fixed stress) for fibrin clots in [47] and [70] is of more value and can be used to corroborate models. Likewise, the pressure gradient-volume flow rate data reported for flow of plasma clots in pipes [103] is also of value while corroborating models.

Over relatively small time scales (10-20 seconds), the rheological behavior of clots (fibrin, plasma or whole blood) is akin to that of a viscoelastic solid, and an enhancement of the elastic modulus (G', see [78] for an explanation of this term) with strain is reported in such experiments (see [8]). Useful data on the fracture strength of whole (human) blood clots (and the variation of this fracture strength with the clot composition) is obtained through such small time scale experiments in [85].

B. Literature survey of models

There are few constitutive models for clots. While there are many studies that characterize the viscoelastic behavior of clots, few develop rigorous non-linear models for them. A linear viscoelastic model of the 3 parameter fluid type was developed in [104] to describe the response of a plasma clot under oscillatory flow conditions. [84] have proposed a 3-D Maxwell model to describe the behavior of coagulating whole blood. The structural parameter in their model was adjusted to fit the time-varying apparent viscosity inferred from steady flow between coaxial cylinders.

C. A viscoelastic liquid model for a coarse ligated plasma clot

A viscoelastic fluid model is developed for describing the behavior of a coarse ligated plasma clot. The properties of this continuum are assumed to depend on, and regulated by the various biochemical processes that take place and this is reflected in the basic balance laws for the continuum being coupled to and augmented by a system of convection-diffusion-reaction equations.

1. Constitutive assumptions

The rate of dissipation ξ associated of the material is defined through

$$\xi = \mathbf{T} \cdot \mathbf{D} - \dot{W} \ , \tag{5.1}$$

where $\mathbf{T}$ denotes the Cauchy stress, W the stored enegy, and ξ the rate of dissipation that is required to be non-negative by virtue of the second law of thermodynamics. The form chosen for the rate of dissipation in the plasma clot is

$$\xi = \alpha^c \Big(\mathbf{D}_{\kappa_{\mathbf{p}(\mathbf{t})}} \cdot \mathbf{B}_{\kappa_{\mathbf{p}(\mathbf{t})}} \mathbf{D}_{\kappa_{\mathbf{p}(\mathbf{t})}} \Big)^{\gamma^c} + \eta_1^c \mathbf{D} \cdot \mathbf{D}. \tag{5.2}$$

The rate of dissipation is set to be non-negative ($\alpha, \eta_1 > 0$) so as to satisfy the second law of thermodynamics.

The Helmholtz potential associated with the elastic response is assumed to be that of a neo-Hookean material:

$$W \equiv \rho\psi = \frac{\mu^c}{2}\left(I_{\mathbf{B}} - 3\right) , \tag{5.3}$$

where ψ is the specific Helmholtz potential, and μ is the shear modulus.

The particular forms for the rate of dissipation and the stored energy correspond to that for a mixture of a viscoelastic fluid that has a power-law viscosity and a Newtonian fluid. Such a choice is appropriate as the plasma clot, that we seek to model, is a mixture of a viscoelastic fluid (the coarse ligated fibrin matrix with bound platelets and the few RBCs, which can aggegate and shear-thin, and WBCs that have not been removed when the plasma is separated from whole blood) and a Newtonian fluid (the entrapped plasma). The viscoelastic fluid model that arises from these constitutive assumptions is the generalized version of a spring-dashpot combination in parallel with a dashpot. The dashpot that is in series with the linear spring is a special dashpot in that its viscosity has a power law dependence on the rate of deformation. The dashpot in parallel is the analog of the Newtonian fluid, and ensures that the resulting model does not exhibit an instantaneous elastic response.

Following the procedure of constrained maximization outlined earlier, the following model is obtained:

$$\mathbf{T} = -p\mathbf{1} + \mathbf{S} , \tag{5.4}$$

$$\mathbf{S} = \mu^c \mathbf{B}_{\kappa_{\mathbf{p}(\mathbf{t})}} + \eta_1^c \mathbf{D} , \tag{5.5}$$

$$\overset{\triangledown}{\mathbf{B}}_{\kappa_{p(t)}} = -2\left(\frac{\mu^c}{\alpha^c}\right)^{1+2n^c}\left(\text{tr}(\mathbf{B}_{\kappa_{\mathbf{p}(\mathbf{t})}}) - 3\lambda\right)^{n^c}\left[\mathbf{B}_{\kappa_{p(t)}} - \lambda\mathbf{1}\right] , \tag{5.6}$$

$$\lambda = \frac{3}{\text{tr}(\mathbf{B}_{\kappa_{\mathbf{p(t)}}}^{-1})}, \tag{5.7}$$

$$n^c = \frac{\gamma^c - 1}{1 - 2\gamma^c}; \quad n^c > 0. \tag{5.8}$$

Here p is a Lagrange multiplier which arises from the requirement that the material be incompressible, and $\mathbf{S}$ is the extra stress tensor.

The notation

$$\mathbf{K}^c = \left(\frac{\mu^c}{\alpha^c}\right)^{1 + 2n^c} \tag{5.9}$$

is introduced for the sake of convenience.

The model equations have the same form as those used to characterize the flow of blood, but the values for the material moduli are different. For instance, the viscosity of the clot can be as much as thirty times that for blood.

D. Model corroboration

A coarse ligated human plasma clot that has been formed in a small tube, one hour after coagulation has been initiated, is modeled. The clot fills the lumen of the entire tube, and is a gel-like material consisting of the fibrin matrix and the entrapped cell matter and plasma. The clot is subject to oscillatory flow with varying amplitudes of pressure gradient applied at a frequency of 2 Hz ([103]), which corresponds to a heart rate of 120 beats per minute. At this frequency, the fibrin matrix (with entrapped fluid) oscillates as one single structure so that modeling it as a single viscoelastic fluid is reasonable (There are, typically, two types of flow when a pressure gradient is applied to a vessel or tube that is filled with a clot: the permeating flow of free fluid through the pores of the clot, and the structural flow of the fibrin matrix with bound fluid. The two flows are sometimes in phase with each other, though not necessarily with the wave form of the applied pressure gradient, depending on the frequency of
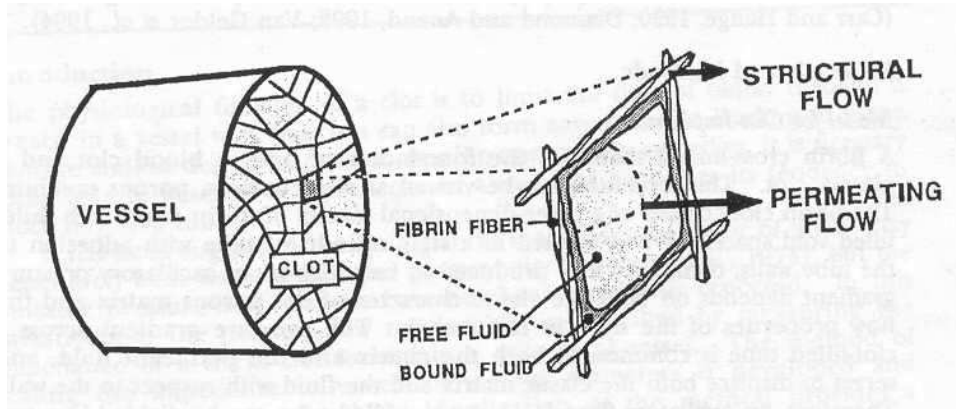
Fig. 14. Flow in a clot-filled vessel; note the two types of flow: permeating, and structural. Reprinted from [104] with permission from IOS Press.

the applied pressure gradient.). The data is in the form of the components of the (amplitude of) applied pressure gradient that are in-phase with, and out-of-phase with, the wave form of the volume flow rate. The component of the pressure gradient that is in phase with the wave form of the volume flow rate is denoted as P', and the component that is out of phase is denoted as P". The model parameters are fixed so that the results from numerical simulations match the experimental data.

1. Application to oscillatory flow

The viscoelastic fluid is subject to an oscillatory pressure gradient of the following form:

$$-\frac{1}{\rho^c}\frac{\partial p}{\partial z} = A\cos(wt) \ . \tag{5.10}$$

A velocity-pressure solution pair of the form:

$$\mathbf{v} = u(r,t)\hat{\mathbf{e}}_z \ , \ \ p = p(r,z,t) \ , \tag{5.11}$$

is sought. A time periodic solution is sought for **v** given that the imposed pressure gradient is time periodic.

Substituting Equations (5.10),(5.11) into the balance of linear momentum and assuming that the components of the stress depend only on the radial coordinate (which is tantamount to specifying the form of the deformation from the instantaneous natural configuration to the current configuration), the following equations are obtained (in non-dimensional form):

$$\frac{\partial u^*}{\partial t^*} = -\frac{\partial p^*}{\partial z^*} + \frac{S^*_{rz}}{r^*} + \frac{\partial S^*_{rz}}{\partial r^*} \ , \tag{5.12}$$

$$\frac{\partial B_{rz}}{\partial t^*} = \frac{\partial u^*}{\partial r^*}B_{rr} - 2\chi(\mathbf{B}_{\kappa_{p(t)}})\frac{R}{\mathsf{Ve}}B_{rz} \ , \tag{5.13}$$

$$\frac{\partial B_{rr}}{\partial t^*} = 2\chi(\mathbf{B}_{\kappa_{p(t)}})\frac{R}{\mathsf{Ve}} (\lambda - B_{rr}) \ , \tag{5.14}$$

$$\frac{\partial B_{zz}}{\partial t^*} = 2\frac{\partial u^*}{\partial r^*}B_{rz} + 2\chi(\mathbf{B}_{\kappa_{p(t)}})\frac{R}{\mathsf{Ve}} (\lambda - B_{zz}) \ , \tag{5.15}$$

where

$$S^*_{rz} = \frac{\mu^c}{\rho^c\mathsf{Ve}^2}B_{rz} + \frac{\eta^c_1}{2\rho^c R\mathsf{Ve}}\frac{\partial u^*}{\partial r^*} \ , \tag{5.16}$$

$$\lambda = \frac{3B_{rr}(B_{rr}B_{zz} - B^2_{rz})}{B^2_{rr} + 2B_{rr}B_{zz} - B^2_{rz}} \ , \tag{5.17}$$

$$\chi(\mathbf{B}_{\kappa_{p(t)}}) = \mathsf{K}^c\Big(2B_{rr} + B_{zz} - 3\lambda\Big)^{n^c} \ , \tag{5.18}$$

and R, Ve are the pipe radius and characteristic velocity respectively. (Note: $B_{\theta\theta} = B_{rr}$, $B_{r\theta} = B_{\theta z} = 0$).

The non-dimensionalisation is as follows: $t^* = t\mathsf{Ve}/R$, $w^* = wR/\mathsf{Ve}$, $u^* = u/\mathsf{Ve}$, $r^* = r/R$, $z^* = z/R$, $S^*_{rz} = S_{rz}/\rho^c\mathsf{Ve}^2$, $p^* = p/\rho\mathsf{Ve}^2$, and $A^* = AR/\mathsf{Ve}^2$ (where $\rho^c = 1025.9$ kg/m^3 is the density of the plasma clot, R = 0.0927 cm as in the experimental set-up, and Ve = 0.001 m/s) .

The above PDEs are solved in the domain 0<r<1, for t≥ 0, subject to the

following boundary condition:

$$u^*(1, t) = 0 , \tag{5.19}$$

and the center-line condition:

$$\frac{\partial u^*(0, t)}{\partial r^*} = 0 . \tag{5.20}$$

The exact solution for oscillatory flow of a Newtonian fluid is used as the initial condition for the velocity profile, whereas $\mathbf{B}_{\kappa_{\mathbf{p(t)}}} = \mathbf{1}$ is used to obtain an initial guess for the components B_{rz}, B_{rr}, B_{zz}.

The (coupled) PDEs are decoupled by treating the PDE for the velocity as an IBVP, while the PDEs for B_{rz}, B_{rr}, B_{zz} are treated as IVPs. The coupling is brought about by means of an iterative process at each time step; the iteration proceeding until consecutive iteratives are within 10^{-4} of each other for all variables. It is enough to fix the boundary conditions for the velocity given the absence of the spatial derivative for B_{rz}, B_{rr} and B_{zz} (the components of $\mathbf{B}_{\kappa_{\mathbf{p(t)}}}$). A Backward-Time, Central-Space (BTCS) scheme is used to discretize the equations ($\Delta r = 0.02$, $\Delta t = 0.0002$), and the resulting system of algebraic equations is solved. The tri-diagonal system of algebraic equations for the velocity are solved by means of a standard Thomas algorithm, and the coupled nonlinear algebraic equations for the components of $\mathbf{B}_{\kappa_{\mathbf{p(t)}}}$ are solved by means of the 'fsolve' routine in MATLAB.

The results for the parameters agree reasonably well with the experimental data (Figure 15). A better agreement with experiments could be achieved by modifying the specific choices for the stored energy and dissipation, but this is not done given the rudimentary nature of the numerical procedures used here.
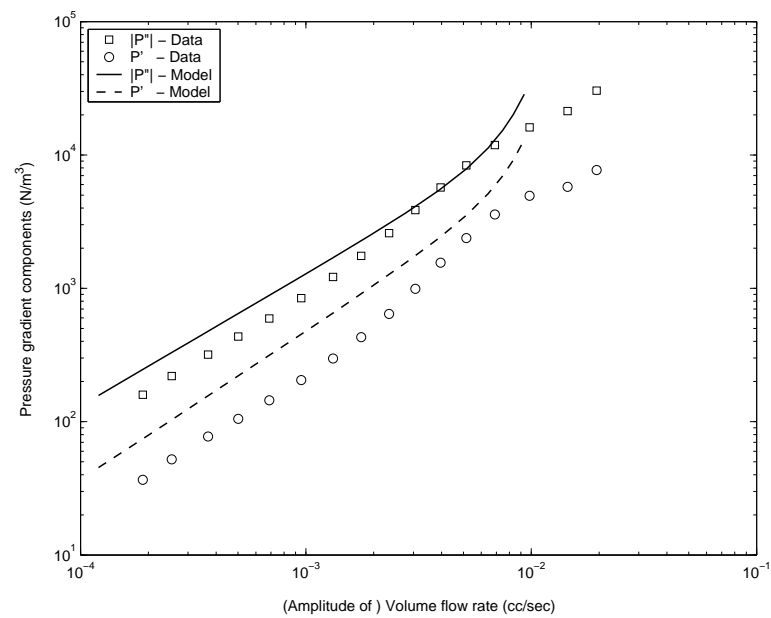
Fig. 15. Comparison of model predictions with experimental data; pressure gradient components that are in and out of phase with the (wave form of) the resulting flow rate; $\mathsf{K}^c = 2.2sec^{-1}$, $\mu^c = 4.9\ N/m^2$, $n^c = 0.1$ and $\eta_1^c = 0.1Pa \cdot s$

E.   Physical relevance of model predictions

The apparent viscosity predicted by the model (the relevant expression has the same form as that for blood flow) at shear rates of $0.06 sec^{-1}$ and $650 sec^{-1}$ is found to be $2.2\ Pa \cdot s$ and $0.0821\ Pa \cdot s$. This is around 30 and 15 times, respectively, the viscosity of human blood at the corresponding shear rates ($0.0736\ Pa \cdot s$ and $0.005\ Pa \cdot s$). This is in keeping with the expectation that the clot be more viscous than blood. The clot is also more viscous (1800 to 70 times higher) than the plasma (viscosity of 0.0012 $Pa \cdot s$) from which it is formed.

In the literature surveyed, no data was found that reported apparent viscosity data for the coarse ligated plasma clot. Experimental considerations come in the way of measurements of the clot response to steady pressure gradients across a pipe. The flow rate is too small to be measured, and when a steady pressure gradient is applied, very soon after the pressure gradient is applied, the entire gel-like structure gives way and releases the entrapped plasma that is not bound to the matrix structure. A discussion of these issues can be found in [4].

CHAPTER VI

APPLICATION OF MODEL FRAMEWORK TO FLOW PROBLEMS,

SUMMARY, AND DIRECTIONS FOR FUTURE STUDY

The elucidation of Virchow's triad requires, firstly, a framework that can pull together the rheological and biochemical changes during the formation and dissolution of clots in flowing blood. Secondly, this framework must be tested in the various flow regimes that are encountered in the vasculature so as to gain an insight into the various factors influencing the phenomenon. The framework consisting of the constitutive model for blood, the convection-diffusion-reaction equations for clot formation and dissolution, and the constitutive model for the plasma clot is tested in three simple flow problems that represent some of the flow regimes that may be encountered in the human vasculature. The equations that need to be solved are generally complex, and require sophisticated numerical procedures. In this dissertation, the full system of equations is solved only for the first flow problem, the equations are formulated but not solved for the second flow problem, and the models for blood and clot are used with a very simple activation criterion in presenting results for the third flow problem. The insights gained from the entire study are then summarized, and directions for future study are suggested.

A. Application of model framework to simple flow problems

The rheological aspects of the phenomenon of clot formation and dissolution in flowing blood have not been considered with the depth that they merit in most mathematical models that have appeared in the literature. Typical simplifying assumptions include using Newtonian models for describing the flow of blood, neglecting the effect of the growing thrombus on the flow itself, or neglecting to describe the rheological behavior

of the clot. A list of studies that have tried to study clot formation and dissolution in flowing blood can be found in [2]. The approach followed here is an attempt to overcome the inaccuracies that may be introduced by such assumptions.

1. Quiescent conditions on a plane

The system of (reaction-diffusion) equations that apply to the case of clot formation and dissolution in quiescent conditions (platelet-poor physiologic plasma) on a plane are solved, and the results for this case are presented.

The model equations, and the solution procedure, have been detailed in an earlier chapter. Only one spatial dimension and time are considered, and the dynamics of the process are investigated over 3600 seconds in a 2 mm domain. The entire set of model equations is studied, with appropriate initial conditions, and boundary conditions picked to account for a simultaneous activation of the extrinsic and intrinsic pathways, and for the fibrinolytic pathway. The equations are solved using the 'pdepe' routine in MATLAB.

The temporal and spatial variations in fibrin (Ia) concentration (tied to the presence or absence of the clot at any point; [Ia] $\geq$ 600 nM implies the presence of a clot) are presented in Figures 16 and 17. The latter provides a value of 5.1 minutes for the time for the initiation of clot formation.

2. Poiseuille-type flow in a cylindrical annulus

The system of equations that apply for the case of clot formation and dissolution in (time-varying) poiseuille-type flow conditions (with constant flow rate) in a cylindrical annulus are presented but they are not solved. The variation in time is due to the fact that although initially only blood flows, the extent of the flow domain, for both blood flow and clot flow, changes as the clot grows and dissolves. This problem
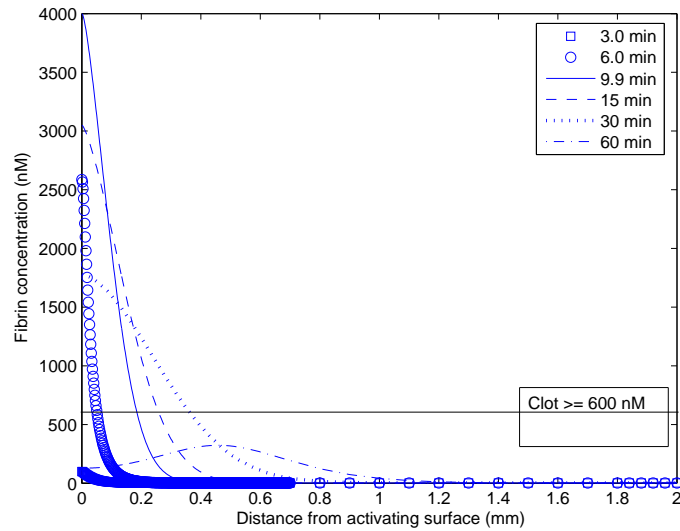
Fig. 16. Temporal evolution of fibrin (Ia) concentration during clot ([Ia] $\geq$ 600 nM) formation, elongation, and dissolution in quiescent platelet-poor plasma on a thrombogenic plane.

has relevance for corroborating the results from the entire framework of models with experimental data for thrombus formation and dissolution on the subendothelium of a human artery/vein exposed to citrated whole human blood [106] in an annular perfusion chamber [11] over a time period of upto 40 minutes. Although the data is for thrombi that are formed non-uniformly on several parts of the exposed surface, it is reduced as if the thrombi were formed all over the surface; i.e. given the data for the percent of the surface covered by thrombi and the average height of the thrombi, a uniform layer of a thrombus of proportional height is assumed to have been formed. Further details concerning the corroboration can be found in [2].

The equations prior to the formation of the clot, when only blood flows, are derived first.
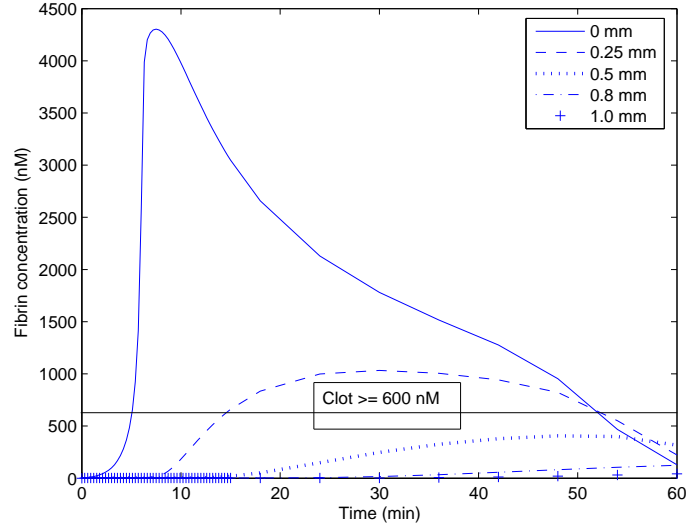
Fig. 17. Spatial evolution of fibrin (Ia) concentration during clot ([Ia] $\geq$ 600 nM) formation, elongation, and dissolution in quiescent platelet-poor plasma on a thrombogenic plane.

A flow field of the following form is assumed to exist at each instant of time 't':

$$\mathbf{v}|_t = u(r)\hat{\mathbf{e}}_z \ , p|_t = p(r, z) \ . \tag{6.1}$$

It is assumed that the displacement field is such that the components of $\mathbf{B}_{\kappa_p(t)}|_t$ are functions of the radial coordinate 'r' alone.

At each instant of time a steady pressure gradient of the form

$$\frac{\partial p}{\partial z}|_t = -C|_t; \ C|_t > 0 \ , \tag{6.2}$$

is applied.

Henceforth, the suffix 't' is dropped for the sake of convenience.

Initially, only blood flows in the annular region. The equations governing the flow, obtained after substituting the model equations for blood into the equation for the balance of linear momentum, are:

$$\frac{du}{dr} = \left(\frac{\partial p}{\partial z} r + \frac{2k_1}{r} \right) \frac{1}{\left(\frac{\mu^b \lambda}{\chi^b} + \eta_1^b \right)} \ , \tag{6.3}$$

where

$$\lambda = \frac{1}{\left[1 + \frac{1}{4(\chi^b)^2} \left(\frac{du}{dr} \right)^2 \right]^{\frac{1}{3}}} \ , \tag{6.4}$$

$$\chi^b = K^b \left[\frac{\lambda}{2(\chi^b)^2} \left(\frac{du}{dr} \right)^2 \right]^{n^b} \ , \tag{6.5}$$

and k_1 is an integration constant that is to be evaluated.

The above equations are to be solved subject to the boundary conditions

$$u(R_i) = 0 \ , \tag{6.6}$$

$$u(R_o) = 0 \ , \tag{6.7}$$

where R_i and R_o are the inner and outer radii of the annular region between the surface of the mounted vessel segment and the wall of the perfusion chamber. The average thickness of the human arterial segment that is mounted is 291μm, and the dimensions of the perfusion chamber ("Original" configuration, see [109]), are $R_i = 0.2036$ cm, $R_o = 0.305$ cm.

The solution has to meet the condition:

$$Q = \int_{R_i}^{R_o} 2\pi r u \, dr = 160 ml/min \ . \tag{6.8}$$

This requires an iterative procedure which is implemented.

Equations (6.3)-(6.7) hold as long as whole blood flows through the perfusion chamber, and clot formation has not been initiated. Clot formation occurs once the threshold boundary condition has been crossed, and the reactions are sufficiently advanced in time. Clot formation occurs on the inner wall, and the clot grows into

the annular gap, reducing the domain where blood flows. The location of the blood-clot interface at a given instant of time($s|_t$) is between, or at, the boundaries of the annulus, i.e., $R_i \leq s|_t \leq R_o$.

A flow field of the following form is assumed to exist at each instant of time 't' for blood:

$$\mathbf{v}^b|_t = u^b(r)\hat{\mathbf{e}}_z \ , p^b|_t = p^b(r, z) \ . \tag{6.9}$$

It is assumed that the displacement field is such that the components of $\mathbf{B}_{\kappa_p(t)}|_t$, for blood, are functions of the radial coordinate 'r' alone.

A steady pressure gradient of the form

$$\frac{\partial p^b}{\partial z}|_t = -C|_t; \ C|_t > 0 \ , \tag{6.10}$$

is applied in the blood zone, and the same pressure gradient is applied in the clot zone as well.

The following equations pertain to the flow of blood:

$$\frac{du^b}{dr} = \left(-C|_t \ r + \frac{2k_1^b}{r}\right) \frac{1}{\left(\frac{\mu^b \lambda^b}{\chi^b} + \eta_1^b\right)} \tag{6.11}$$

where

$$\lambda^b = \frac{1}{\left[1 + \frac{1}{4(\chi^b)^2}(\frac{du^b}{dr})^2\right]^{\frac{1}{3}}} \ , \tag{6.12}$$

$$\chi^b = K^b\left[\frac{\lambda^b}{2(\chi^b)^2}(\frac{du^b}{dr})^2\right]^{n^b} \ , \tag{6.13}$$

and k_1^b is an integration constant that is to be evaluated. These equations are solved subject to the boundary conditions

$$u^b(s|_t) \ = \ U_{INT} \ , \tag{6.14}$$

$$u^b(R_o) \;=\; 0 \; . \tag{6.15}$$

A flow field of the following form is assumed to exist at each instant of time 't' for the clot:

$$\mathbf{v}^c|_t = u^c(r)\hat{\mathbf{e}}_z \; , \; p^c|_t = p^c(r,z) \; . \tag{6.16}$$

It is assumed that the displacement field is such that the components of $\mathbf{B}_{\kappa_p(t)}|_t$, for the clot, are functions of the radial coordinate 'r' alone.

A steady pressure gradient of the form

$$\frac{\partial p^c}{\partial z}|_t = -C|_t; \; C|_t > 0 \; , \tag{6.17}$$

is applied in the clot zone; this pressure gradient is the same as that applied for blood flow.

The equations pertaining to the flow of the clot (obtained after substituting the model equations for the clot in the equation for the balance of linear momentum) are:

$$\frac{du^c}{dr} = \left(-C|_t \, r + \frac{2k_1^c}{r} \right) \frac{1}{\left(\frac{\mu^c \lambda^c}{\chi^c} + \eta_1^c \right)} \tag{6.18}$$

where

$$\lambda^c = \frac{1}{\left[1 + \frac{1}{4(\chi^c)^2}(\frac{du^c}{dr})^2 \right]^{\frac{1}{3}}} \; , \tag{6.19}$$

$$\chi^c = K^c \left[\frac{\lambda^c}{2(\chi^c)^2}(\frac{du^c}{dr})^2 \right]^{n^c} \; , \tag{6.20}$$

and k_1^c is an integration constant that is to be evaluated. These equations are solved subject to the boundary conditions

$$u^c(R_i) \;=\; 0 \; , \tag{6.21}$$

$$u^c(s|_t) \;=\; U_{INT} \; . \tag{6.22}$$

In addition to solving the two sets of equations for the flow of blood and the flow of clot, for a given pressure gradient $-C|_t$, the following conditions are to be satisfied for the balance of mass and linear momentum across the interface:

$$u^b(s|_t) \quad = \quad u^c(s|_t) = U_{INT} \ , \tag{6.23}$$

$$T_{rz}^b(s|_t) \quad = \quad T_{rz}^c(s|_t) \ , \tag{6.24}$$

$$T_{rr}^b(s|_t) \quad = \quad T_{rr}^c(s|_t) \ . \tag{6.25}$$

The density change between blood and clot is neglected in formulating these conditions. This seems reasonable given that the density of human blood (ρ^b) is 1.05 g/cc, and the density of a human plasma clot (ρ^c) is 1.03 g/cc.

In addition, the solution has to meet the condition:

$$Q = \int_{R_i}^{s|_t} 2\pi r u^c dr + \int_{s|_t}^{R_o} 2\pi r u^b dr = 160 ml/min \ . \tag{6.26}$$

The solution of the blood-clot problem at each instant of time 't', requires two levels of iteration: One until the conditions in Equations (6.23)-(6.25) are met, and the other until the condition in Equation (6.26) is met. This procedure is to be implemented.

3. Oscillatory flow in a rigid-walled pipe

The system of equations that apply for the case of clot formation and dissolution during oscillatory flow in an infinitely long rigid-walled cylindrical pipe (of radius 'R') are too difficult to be solved, and so a very simple activation criterion (in place of the convection-diffusion-reaction equations and the corresponding criteria) is used to denote the switch between the model for blood (referred to as Model 1) and the model for clot (referred to as Model 2); the results yield qualitative insights into the

results that may be obtained with a larger system of equations.

The model used for blood (Model 1) is the same as that outlined in an earlier chapter. The parameters for Model 1 are: $K^1 = 1.2056sec^{-1}$, $\mu^1 = 0.0227\ Pa$, $n^1 = 0.7525$ and $\eta_1^1 = 0.01Pa \cdot s$. The density of this liquid is $\rho^1 = 1050\ kg/m^3$.

The switch in models between that of blood and that of clot, or activation, is said to take place upon prolonged exposure to shear stresses above a threshold value (T_{cr}). This mimics platelet activation and subsequent aggregation (and, thus, thrombus formation) upon exposure to supra-threshold shear stresses ($\geq T_{cr}$), and is a very simplistic view of thrombus formation; however, it is entirely possible that such a situation is encountered in the circulatory system. To quantify the idea of activation due to prolonged exposure to supra-threshold shear stresses, a phenomenological activation number, $B(t)$, is defined (Equation 6.27) and associated of each platelet. The initial state of the platelets, or the resting platelet, is set to an activation number of zero (i.e. $B(0) = 0$). The activation number is defined as follows:

$$B(t) \ = \ B(0) + \frac{1}{B_0} \int_0^t e^{k\left(\frac{|\tau_{rz}|}{T_{cr}}-1\right)} H(|\tau_{rz}| - T_{cr}) dt \qquad (6.27)$$

$$H(|\tau_{rz}| - T_{cr}) \ = \ \begin{cases} 1 & |\tau_{rz}| \geq T_{cr} \\ 0 & |\tau_{rz}| < T_{cr} \end{cases} \qquad (6.28)$$

The activation number can either increase or stay constant reflecting exposure to time varying shear stresses that are or are not above the threshold value (T_{cr}), and platelet activation occurs when a threshold activation number B_{thr} is reached. Activated platelets are lysed if the activation number exceeds a critical value, B_{damage}, in the time period t_{act} that it takes for the resting platelet to be activated. In the special flow field that is considered, it is quite easy to track the activation of platelets by just verifying the activation number at each point in the flow domain. The idea of quantifying, and tracking, platelet activation by means of $B(t)$ is based on the

damage accumulation criterion introduced in [123]. The application to the problem of clot formation and dissolution is a novelty, however, and this is outlined below.

The criterion for activation and the subsequent use of Model 2 for the clot in regions where we initially employed Model 1 for blood is:

$$\text{If } B(t - t_{act}) > B_{thr} \text{ and } B(t) < B_{damage} \ , \tag{6.29}$$

$$\text{Or } B(t - t_{act}) = B_{thr}, \dot{B}(t - t_{act}) > 0 \text{ and } B(t) < B_{damage} \ , \tag{6.30}$$

$$\text{Then Model} = \text{Model2} \ . \tag{6.31}$$

The criterion for dissolution and the subsequent use of Model 1 where the clot has dissociated is:

$$\text{If } B(t - t_{act}) > B_{thr} \text{ and } B(t) > B_{damage} \ , \tag{6.32}$$

$$\text{Then Model} = \text{Model1} \ . \tag{6.33}$$

The parameters for the activation criterion are $B_0 = 300$s, $t_{act} = 0.02$s, k $= 0.75$, $T_{cr} = 1 \ Nm^{-2}$, $B_{thr} = 0.0004$, $B_{damage} = 1$.

The model used for the clot (Model 2) has the same form as that outlined in an earlier chapter.

The parameters for Model 2 are: $\mathsf{K}^2 = 1.2056 sec^{-1}$, $\mu^2 = 0.0227 \ Pa$, $n^2 = 0.7525$ and $\eta_1^2 = 0.04 Pa \cdot s$; Note that the viscosity term η_1^2 for Model 2 is four times the viscosity term η_1^1 for Model 1, i.e., the clot while also a viscoelastic liquid is four times more viscous than blood. The density of this liquid is $\rho^2 = 1050 \ kg/m^3$.

The development of the equations governing this problem is very similar to the development of the equations governing time-varying poiseuille-type flow in a cylindrical annulus, in so-far as the boundary conditions for the domains occupied by blood and clot and the conditions to be met at the blood-clot interface. The only difference
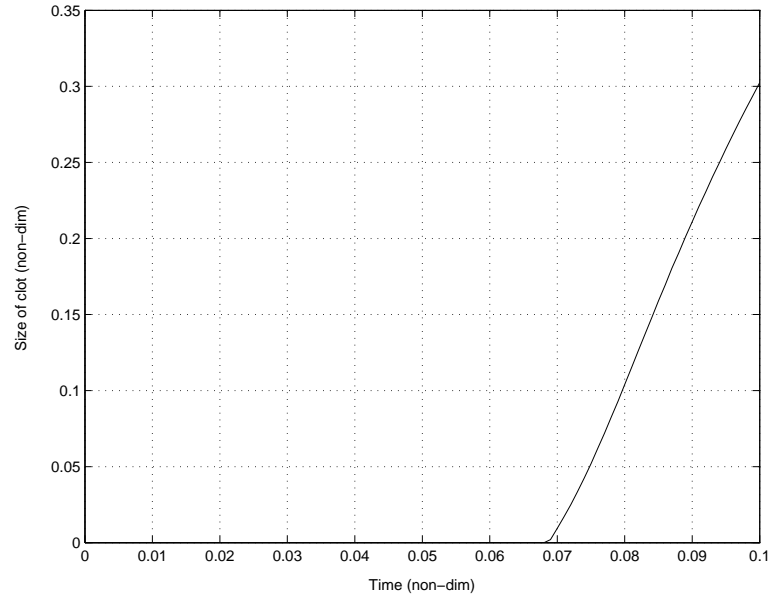
Fig. 18. Increase of size of domain of the clot (described by Model 2) $(1 - s^*|_t)$ with time (R = 0.005m)

is that the fluids are subject to an oscillatory pressure gradient, and the equations that govern the flow of blood and clot are those for oscillatory flow (these have been developed in earlier chapters). Further details pertaining to the development of the equations can be found in [2].

The following results are obtained for the moving boundary problem that has been outlined. Figure 18 tracks the location of $s^*|_t$ in time. Figures 19 through 22 document the velocity, shear stress (Note the steep increase in shear stress in the region occupied by the clot), and normal stresses (B_{rr} and B_{zz}) at t = 0.05 sec after the onset of oscillatory flow. Figure 23 documents the variation of centerline velocity in the course of the 0.05 sec after the onset of oscillatory flow.
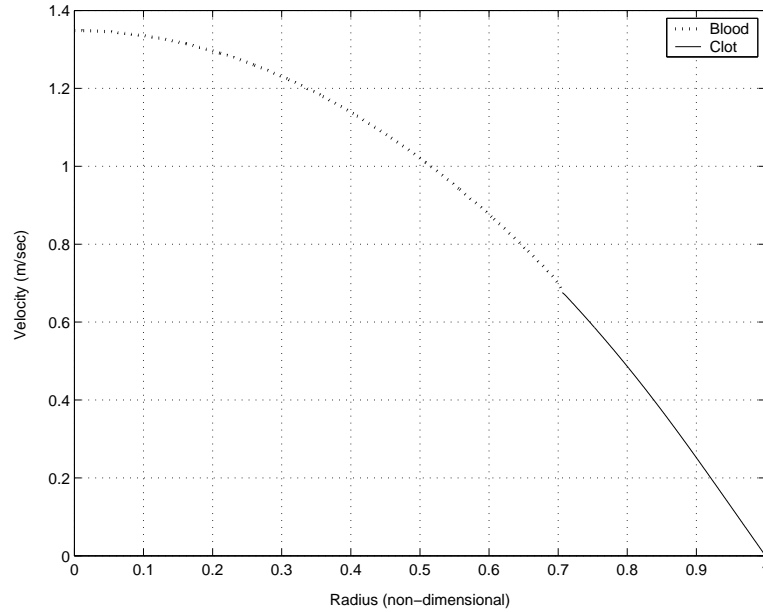
Fig. 19. Predictions of blood-clot velocity profile (moving boundary, oscillatory flow) at t = 0.05 sec ($t^* = 0.1$)

B. Summary

A framework of models for the elucidation of Virchow's triad has been presented. The framework consists in a model for the rheological behavior of blood, convection-diffusion-reaction equations to incorporate the rheological influences on, the biochemical changes during, and the surface modulation of the formation and dissolution of clots, and a model for the rheological behavior of the clot that is formed.

The model characterizing the rheological behavior of human blood is developed in a theory with a firm thermodynamic basis, and is the first to incorporate the shear-thinning attributes, and the *deformation-dependent* viscoelastic behavior of blood. The model is corroborated under a set of conditions representative of flow regimes that are present in the human vasculature, and its predictions for flow reversals under

Fig. 20. Predictions of blood-clot shear stress profile (moving boundary, oscillatory flow) at t = 0.05 sec ($t^* = 0.1$)
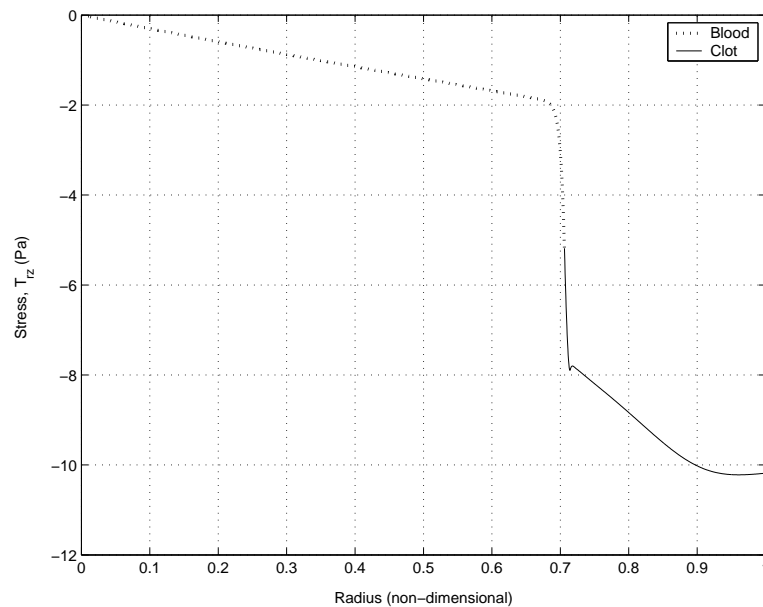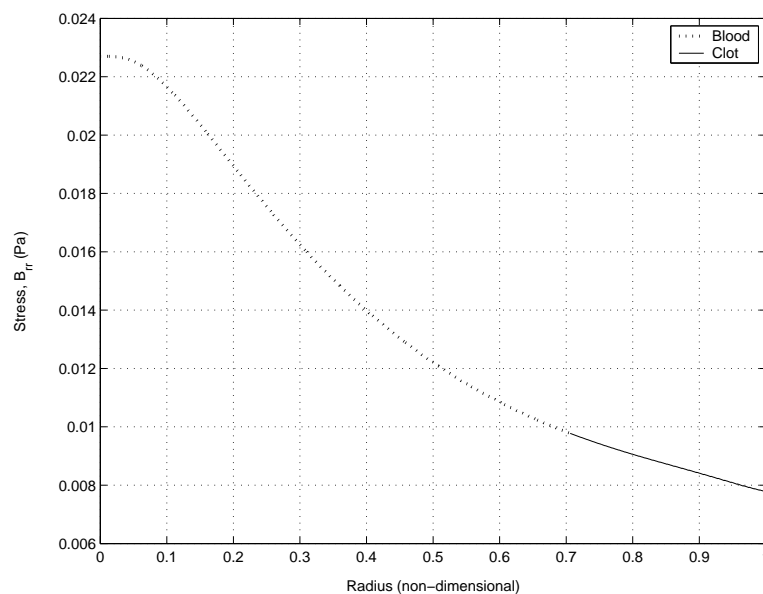

Fig. 21. Predictions of blood-clot radial normal stress (Brr) profile (moving boundary, oscillatory flow) at t = 0.05 sec ($t^* = 0.1$)
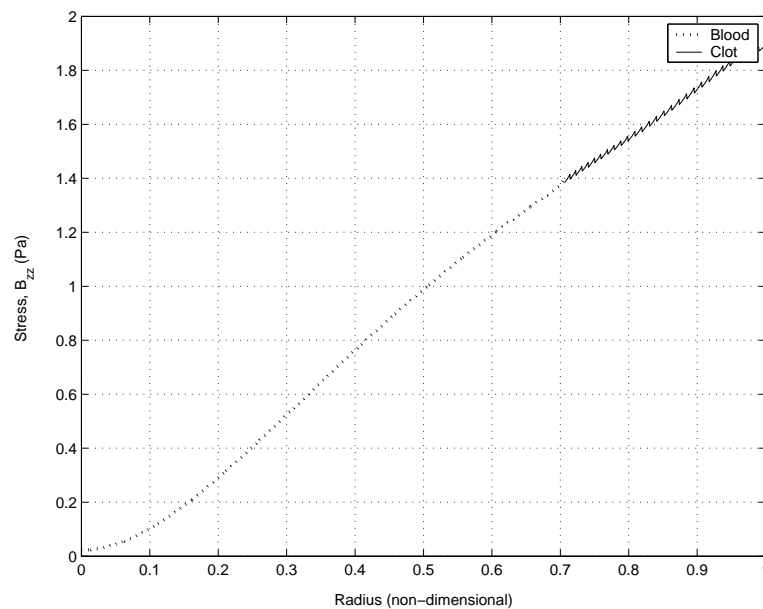
Fig. 22. Predictions of blood-clot axial normal stress (Bzz) profile (moving boundary, oscillatory flow) at t = 0.05 sec $(t^* = 0.1)$
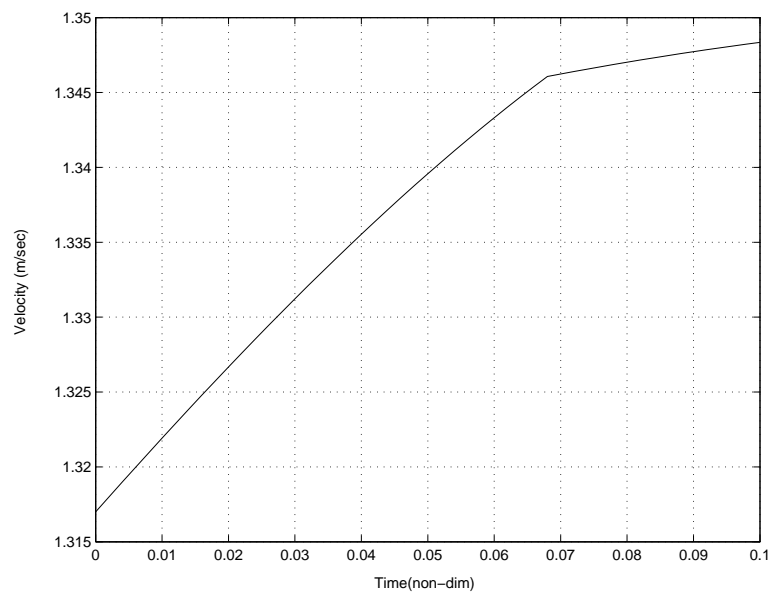

Fig. 23. Variation of centerline velocity with time; oscillatory flow, Blood-clot moving boundary problem

pulsatile flow conditions represent an interesting consequence of the experimentally observed fact that the viscoelastic-behavior of blood is less prominent at high shear rates (where the Newtonian behavior dominates).

The convection-diffusion-reaction equations represent a unifying link that helps bring together the legs of Virchow's triad in a manner that is conducive to numerical testing under various flow regimes that are of relevance to the development of cardio-vascular devices. The reaction-diffusion equations are corroborated with experimental data for clot formation, and clot dissolution in quiescent plasma derived from human blood. The model predictions for the severity of Antithrombin-III deficiency over Protein-C deficiency tie in nicely with clinical data, and, with the detailed documentation of the results that is being given in the paper under preparation [3], represent a positive result for the development of mathematical models (for hemostasis) that have predictive capability.

The model characterizing the rheological behavior of the clot formed from human plasma has a rigorous thermodynamic basis, and represents a clear improvement over earlier models in that it can describe the non-linear viscoelastic response of the clot. The model is corroborated under conditions representative of flow regimes present in the vasculature (arterial-type flow), and its predictions of large apparent viscosities are in keeping with the physical expectation that the clot be more viscous than blood.

The framework of models is tested in three simple flow regimes representative of conditions in the vasculature. The simulations are performed for the case of quiescent conditions in a pool of plasma on a plane, and the results for the growth and dissolution of clot are in keeping with an intuitive expectation of the process. The equations for the case of time-varying poiseuille-type flow in a cylindrical annular region are presented but they are not solved. The case of oscillatory flow in a rigid-walled cylindrical pipe is studied albeit with a simplified set of models, and the results

for the growth of the clot lend insights into the phenomenon. The centerline velocity drops as the clot grows which keeps with physical expectation, and the shear-stresses encountered in the region of the clot suggest that clot rupture could be abrupt (i.e. thrombo-embolization could occur) under certain flow conditions.

C.   Directions for future study

There are several limitations that need to be addressed with each component of the framework and also with the testing in flow problems, and extensions can be made in several directions.

The constitutive model for blood treats blood as a homogenized continuum, and has the inherent limitation that one cannot infer the distribution of the individual components during the flow, nor can the interaction between these components be inferred. A first step in this direction would be the development of a mixture theory model for blood that has separate constitutive equations for RBCs, and plasma, and constitutive specifications for the interaction between these components. Another issue with the model for blood is that the choice for the rate of dissipation and the stored energy function necessitates the introduction of the Heaviside function to address the issue of the zero-shear viscosity. This is a cumbersome detail, and a better choice for the rate of dissipation and stored energy function must be made to address this issue. One step in this direction would be to explore making a choice for the rate of dissipation that corresponds to a generalized-Maxwell *and* a generalized-Newtonian (power-law) liquid. Such a choice would make the model easier for mathematical analysis. The model for blood is also limited in that the effect of hematocrit on the property variations is not incorporated, and steps in this direction should be taken.

The convection-diffusion-reaction equations for the formation and dissolution of

clots in flowing blood represent an initial attempt to develop a model incorporating the relevant mechanical and biochemical changes during the complete process. This model is, by no means, comprehensive, and several constituents (like f-VII, f-XIII, Protein S, etc.) and details concerning their interactions (like the incorporation of separate binding sites for enzyme complexes on the membrane of activated platelets) need to be added to lend completeness to the model. A discussion on some of the steps that can be implemented to extend these equations is found in [2].

The constitutive model for the clot suffers from some of the same limitations as the model for blood in that it treats a porous fibrin matrix bound to platelets and permeated by entrapped plasma as a homogenized continuum. The interactions between the constituents, though highly relevant for oscillatory and pulsatile flow, cannot be captured by means of this approach. A first step to address this limitation would be the development of a mixture theory model for the clot with separate constitutive equations for the fibrin matrix and the RBC-platelet-plasma aggregate and constitutive specifications for the interactions between them. The variation of clot properties with factors like the age of the clot, the extent of ligation, and the pH during formation are also steps that should be taken. In addition, the clot properties could be tied to the progress of the fibrin polymerization reactions (something which is not done right now). As such, of course, the results obtained during the model corroboration seem to suggest that a different choice for the rate of dissipation and the stored energy function would yield a better fit with the experimental data, apart from redressing the rather cumbersome detail of the Heaviside function that is introduced right now.

The testing of the framework in the simple flow problems opens up several numerical issues that need to be addressed if reliable results and, thus, a better understanding of the phenomenon are to be obtained. The entire set of equations from

using the framework of models need to be solved for both the time-varying poiseuille-type flow, and also for the case of the oscillatory flow in a rigid-walled pipe. The results from these studies would, hopefully, shed insight into, among other facets of the phenomenon, the manner of clot dissolution (whether gradual or abrupt, and the probability of thrombo-embolisms being formed). An ambitious step for the future would be to apply the framework to the complex flow geometry of a heart pump; such a study would be a key facet in the development of reliable cardiovascular devices that can be used to reduce the suffering of patients.

REFERENCES

[1] AHMAD, S. S., RAWALASHEIKH, R., & WALSH, P. N. Comparative interactions of factor-IX and factor-IXa with human platelets. *Journal of Biological Chemistry* **264** (1989), 3244–3251.

[2] ANAND, M., RAJAGOPAL, K., & RAJAGOPAL, K. R. A model incorporating some of the mechanical and biochemical factors underlying clot formation and dissolution in flowing blood. *Journal of Theoretical Medicine* **5** (2003), 183–218.

[3] ANAND, M., RAJAGOPAL, K., & RAJAGOPAL, K. R. A model for the formation and dissolution of clots in quiescent platelet-poor plasma on exposure to a thrombogenic surface. an insight into the clinical observations of the severity of AT-III deficiency over Protein-C deficiency. (In Preparation).

[4] ANAND, M., RAJAGOPAL, K., & RAJAGOPAL, K. R. A viscoelastic liquid model for describing the flow of a coarse ligated plasma clot. (Accepted). *Theoretical and Computational Fluid Dynamics* (2005).

[5] ANAND, M., & RAJAGOPAL, K. R. A shear-thinning viscoelastic fluid model for describing the flow of blood. *International Journal of Cardiovascular Medicine and Science* **4** (2004), 59–68.

[6] ATAULLAKHANOV, F. I., ZARNITSINA, V. I., POKHILKO, A. V., LOBANOV, A. I., & MOROZOVA, O. L. Spatio-temporal dynamics of blood coagulation and pattern formation. a theoretical approach. *International Journal of Bifurcation and Chaos* **12** (2002), 1985–2002.

[7] BALASUBRAMANIAN, V., GRABOWSKI, E., BINI, A., & NEMERSON, Y. Platelets, circulating tissue factor, and fibrin colocalize in ex vivo thrombi:

real-time fluorescence images of thrombus formation and propagation under defined flow conditions. *Blood* **100** (2002), 2787–2792.

[8] BALE, M. D., & FERRY, J. D. Shear enhancement of elastic modulus in fine fibrin clots. *Thrombosis Research* **52** (1988), 565–572.

[9] BAUER, K. A. Hypercoagulable states. In: R. Hoffman, E. J. Benz, S. J. Shattil, B. Furie, H. J. Cohen, L. E. Silberstein, and P. McGlave, (eds), *Hematology : Basic principles and practice*, 3rd ed. pp. 2009–2039. Churchill Livingstone, Philadelphia (2000).

[10] BAUER, K. A., & ROSENBERG, R. G. Control of coagulation reactions. In: E. Beutler, M. A. Lichtman, B. S. Coller, and T. J. Kipps, (eds), *Williams Hematology*, 5th ed. pp. 1239–1251. McGraw Hill Inc., New York (1995).

[11] BAUMGARTNER, H. R. The role of blood flow in platelet adhesion, fibrin deposition and formation of mural thrombi. *Microvascular Research* **5** (1973), 167–179.

[12] BLÖMBACK, B. Fibrinogen and fibrin-proteins with complex roles in hemostasis and thrombosis. *Thrombosis Research* **83** (1996), 1–75.

[13] BLÖMBACK, B., & OKADA, M. Fibrin gel structure and clotting time. *Thrombosis Research* **25** (1982), 51–70.

[14] BOOTH, N. A. Fibrinolysis and thrombosis. *Baillière's Clinical Haematology* **12** (1999), 423–433.

[15] BUNGAY, S. D., GENTRY, P. A., & GENTRY, R. D. A mathematical model of lipid-mediated thrombin generation. *Mathematical Medicine and Biology* **20** (2003), 105–129.

[16] BURGREEN, G. W., ANTAKI, J. F., WU, Z. J., & HOLMES, A. J. Computational fluid dynamics as a development tool for rotary blood pumps. *Artificial Organs* **25** (2001), 336–340.

[17] BUTENAS, S., VANT VEER, C., & MANN, K. G. Normal thrombin generation. *Blood* **94** (1999), 2169–2178.

[18] CARR, M. E., & HERMANS, J. Size and density of fibrin fibers from turbidity. *Macromolecules* **11** (1978), 46–50.

[19] CASSON, N. A flow equation for pigment-oil suspensions of the printing ink type. In *Rheology of disperse systems* (1959), C. C. Mill, (ed), , British Society of Rheology, Pergamon Press, pp. 84–104.

[20] CHARM, S., & KURLAND, G. Viscometry of human blood for shear rates of 0-100,000 sec^{-1}. *Nature* **206** (1965), 617–618.

[21] CHATURANI, P., BISWAS, D., & MAHAJAN, S. P. Reply to the comments on - a two-fluid model for blood flow through small diameter tubes. *Biorheology* **20** (1983), 807–809.

[22] CHATURANI, P., & UPADHYA, V. S. A two-fluid model for blood flow through small diameter tubes. *Biorheology* **16** (1979), 109–118.

[23] CHIEN, S., SUNG, K. L. P., SKALAK, R., USAMI, S., & TÒZEREN, A. L. Theoretical and experimental studies on viscoelastic properties of erythrocyte membrane. *Biophysical Journal* **24** (1978), 463–487.

[24] CHIEN, S., USAMI, S., DELLENBACK, R. J., & GREGERSEN, M. I. Blood viscosity : Influence of erythrocyte aggregation. *Science* **157** (1967), 829–831.

[25] CHIEN, S., USAMI, S., DELLENBACK, R. J., & GREGERSEN, M. I. Blood viscosity : Influence of erythrocyte deformation. *Science* **157** (1967), 827–829.

[26] CHIEN, S., USAMI, S., TAYLOR, H. M., LUNDBERG, J. L., & GREGERSEN, M. I. Effect of hematocrit and plasma proteins on human blood rheology at low shear rates. *Journal of Applied Physiology* **21** (1966), 81–87.

[27] CHO, Y. I., & KENSEY, K. R. Effects of the non-newtonian viscosity of blood on flows in a diseased arterial vessel. 1. steady flows. *Biorheology* **28** (1991), 241–262.

[28] COLMAN, R. W., CLOWES, A. W., GEORGE, J. N., HIRSH, J., & MARDER, V. J. Overview of hemostasis. In: R. W. Colman, J. Hirsh, V. J. Marder, A. W. Clowes, and J. N. George, (eds), *Hemostasis and Thrombosis*, 4th ed. pp. 1–16. Lippincott, Williams and Wilkins (2001).

[29] COPLEY, A. L., & KING, R. G. On the viscoelasticity of anticoagulated whole human blood in steady shear as tested by rheogoniometric measurements of normal forces. *Biorheology* **12** (1976), 5–10.

[30] CROSS, M. M. Rheology on non-newtonian fluids: a new flow equation for pseudoplastic systems. *Journal of Colloid Science* **20** (1965), 417–437.

[31] DAVIE, E. W., & RATNOFF, O. D. Waterfall sequence for intrinsic blood clotting. *Science* **145** (1964), 1310–1312.

[32] DIAMOND, S. L., & ANAND, S. Inner clot diffusion and permeation during fibrinolysis. *Biophysical Journal* **65** (1993), 2622–2643.

[33] EATON, D., RODRIGUEZ, H., & VEHAR, G. A. Proteolytic processing of human factor VIII: correlation of specific cleavages by thrombin, factor Xa, and

activated protein C with activation and inactivation of factor VIII coagulant activity. *Biochemistry* **25** (1986), 505–512.

[34] EVANS, E. A., & HOCHMUTH, R. M. Membrane viscoelasticity. *Biophysical Journal* **16** (1976), 1–11.

[35] FERRY, J. D., & MORRISON, P. R. Preparation and properties of serum and plasma proteins. VIII. the conversion of human fibrinogen to fibrin under various conditions. *Journal of the American Chemical Society* **69** (1947), 388–400.

[36] FREYSSINET, J. M., ORFANOUDAKIS, F. T., RAVANAT, C., GRUNEBAUM, L., GAUCHY, J., CAZENAVE, J. P., & WIESEL, M. L. The catalytic role of anionic phospholipids in the activation of protein c by factor Xa and expression of its anticoagulant function in human plasma. *Blood coagulation and fibrinolysis* **2** (1991), 691–698.

[37] FURIE, B., & FURIE, B. C. Molecular basis of blood coagulation. In: R. Hoffman, E. J. Benz, S. J. Shattil, B. Furie, H. J. Cohen, L. E. Silberstein, and M. P., (eds), *Hematology : Basic principles and practice*, 3rd ed. pp. 1783–1804. Churchill Livingstone, Philadelphia (2000).

[38] GAILANI, D., & BROZE, G. J. Factor XI activation in a revised model of blood coagulation. *Science* **253** (1991), 909–912.

[39] GERTH, C., ROBERTS, W. W., & FERRY, J. D. Rheology of fibrin clots II. linear viscoelastic behavior in shear creep. *Biophysical Chemistry* **2** (1974), 208–217.

[40] Gimbrone, M. A. Endothelial dysfunction, hemodynamic forces and atherosclerosis. *Thrombosis and Haemostasis* **82** (1999), 722–726.

[41] Glover, C. J., McIntire, L. V., Brown, C. H., & Natelson, E. A. Dynamic coagulation studies: Influence of normal and abnormal platelets on clot structure formation. *Thrombosis Research* **7** (1975), 185–198.

[42] Glover, C. J., McIntire, L. V., Brown, C. H., & Natelson, E. A. Rheological properties of fibrin clots. effects of fibrinogen concentration, factor XIII deficiency, and factor XIII inhibition. *Journal of Laboratory and Clinical Medicine* **86** (1975), 644–656.

[43] Goldsmith, H. L., & Turitto, V. T. Rheological aspects of thrombosis and haemostasis: Basic principles and applications. *Thrombosis and Haemostasis* **55** (1986), 415–435.

[44] Hartert, H. H. The proper phase of coagulation. Its physical differentiation by resonance-thrombography and thromboelastography. *Clinical Hemorheology* **2** (1982), 51–69.

[45] Heeb, M. J., Bischoff, R., Courtney, M., & Griffin, J. H. Inhibition of activated protein c by recombinant α_1-antitrypsin variants with substitution of arginine or leucine for methionine. *Journal of Biological Chemistry* **265** (1990), 2365–2389.

[46] Humphrey, J. D. *Cardiovascular Solid Mechanics : Cells, Tissues, and Organs.* Springer Verlag, Heidelberg (2002).

[47] Janmey, P. A., Amis, E. J., & Ferry, J. D. Rheology of fibrin clots. vi. stress relaxation, creep, and differential dynamic modulus of fine clots in large

shearing deformations. *Journal of Rheology* **27** (1983), 135–153.

[48] JONES, K. C., & MANN, K. G. A model for the tissue factor pathway to thrombin. II. a mathematical simulation. *Journal of Biological Chemistry* **269** (1994), 23367–23373.

[49] KAIBARA, M. Rheological studies on blood coagulation and network formation of fibrin. *Polymer Gels and Networks* **2** (1994), 1–28.

[50] KARSAN, A. L., & HARLAN, J. M. The blood vessel wall. In: R. Hoffman, E. J. Benz, S. J. Shattil, B. Furie, H. J. Cohen, L. E. Silberstein, and M. P., (eds), *Hematology : Basic principles and practice*, 3rd ed. pp. 1770–1782. Churchill Livingstone, Philadelphia (2000).

[51] KHANIN, M. A., & SEMENOV, V. V. A mathematical model of the kinetics of blood coagulation. *Journal of Theoretical Biology* **136** (1989), 127–134.

[52] KLINE, K. A. On a liquid drop model of blood rheology. *Biorheology* **9** (1972), 287–299.

[53] KLINE, K. A., ALLEN, S. J., & DESILVA, C. N. A continuum approach to blood flow. *Biorheology* **5** (1968), 111–118.

[54] KOLEV, K., LERANT, I., TENEKEJIEV, K., & MACHOVICH, R. Regulation of fibrinolytic activity of neutrophil leukocyte elastase, plasmin, and miniplasmin by plasma protease inhibitors. *Journal of Biological Chemistry* **269** (1994), 17030–17034.

[55] KRISHNASWAMY, S., CHURCH, W. R., NESHEIM, M. E., & MANN, K. G. Activation of human prothrombin by human prothrombinase. Influence of factor

Va on the reaction mechanism. *Journal of Biological Chemistry* **262** (1987), 3291–3299.

[56] KROLL, M. H., HELLUMS, J. D., McINTIRE, L. V., SCHAFER, A. I., & MOAKE, J. L. Platelets and shear stress. *Blood* **88** (1996), 1525–1541.

[57] KUHARSKY, A. L., & FOGELSON, A. L. Surface mediated control of blood coagulation: the role of binding site densities and platelet deposition. *Biophysical Journal* **80** (2001), 1050–1074.

[58] LASSLO, A. *Blood Platelet Function and Medicinal Chemistry.* Elsevier Biomedical, New York (1984).

[59] LEIPOLD, R. J., BOZARTH, T. A., RACANELLI, A. L., & DICKER, I. B. Mathematical model of serine protease inhibition in the tissue factor pathway to thrombin. *Journal of Biological Chemistry* **270** (1995), 25383–25387.

[60] LEVINE, S. N. Enzyme amplifier kinetics. *Science* **152** (1966), 651–653.

[61] LIJNEN, H. R., & COLLEN, D. Molecular and cellular basis of fibrinolysis. In: R. Hoffman, E. J. Benz, S. J. Shattil, B. Furie, H. J. Cohen, L. E. Silberstein, and M. P., (eds), *Hematology : Basic principles and practice*, 3rd ed. pp. 1804–1814. Churchill Livingstone, Philadelphia (2000).

[62] LOWE, G. D. O. Rheological influences on thrombosis. *Baillière's Clinical Haematology* **12** (1999), 435–449.

[63] MACFARLANE, R. G. An enzyme cascade model in the blood clotting mechanism, and its function as a biochemical amplifier. *Nature* **202** (1964), 498–499.

[64] MADISON, E. L., COOMBS, G. S., & COREY, D. R. Substrate-specificity of tissue-type plasminogen-activator - characterization of the fibrin-dependent

specificity of T-PA for plasminogen. *Journal of Biological Chemistry* **270** (1995), 7558–7562.

[65] MANN, K. G. The assembly of blood clotting complexes on membranes. *Trends in Biochemical Sciences* **12** (1987), 229–233.

[66] MANN, K. G., GAFFNEY, D., & BOVILL, E. G. Molecular biology, biochemistry, and lifespan of plasma coagulation factors. In: B. E., (ed), *Williams Hematology*, 5th ed. pp. 1206–1226. McGraw Hill Inc. (1995).

[67] MARTINELLI, I., MANNUCCI, P. M., STEFANO, V. D., TAIOLI, E., ROSSI, V., CROSTI, F., PACIARONI, K., LEONE, G., & FAIONI, E. M. Different risks of thrombosis in four coagulation defects associated with inherited thrombophilia: A study of 150 families. *Blood* **92** (1998), 2068–2071.

[68] MCMILLAN, D. E., UTTERBACK, N. G., NASRINASRABADI, M., & LEE, M. M. An instrument to evaluate the time dependent flow properties of blood at moderate shear rates. *Biorheology* **23** (1986), 63–74.

[69] MONKOVIC, D. D., & TRACY, P. B. Functional characterization of human platelet-released factor V and its activation by factor Xa and thrombin. *Journal of Biological Chemistry* **265** (1990), 17132–17140.

[70] NELB, G. W., GERTH, C., FERRY, J. D., & LORAND, L. Rheology of fibrin clots. III. shear creep and creep recovery of fine ligated and coarse unligated clots. *Biophysical Chemistry* **5** (1976), 377–387.

[71] NELB, G. W., KAMYKOWSKI, G. W., & FERRY, J. D. Rheology of fibrin clots. V. shear modulus, creep, and creep recovery of fine unligated clots. *Biophysical Chemistry* **13** (1981), 15–23.

[72] NESHEIM, M. E., & FREDENBURGH, J. An experimental and mathematical model for fibrinolysis. *FASEB Journal* **2** (1988), A1412–A1412.

[73] NESHEIM, M. E., TRACY, R. P., & MANN, K. G. "Clotspeed," a mathematical simulation of the functional properties of prothrombinase. *Journal of Biological Chemistry* **259** (1984), 1447–1453.

[74] NEUENSCHWANDER, P. F., & JESTY, J. Thrombin-activated and factor Xa-activated human factor VIII: Differences in cofactor activity and decay rate. *Archives of Biochemistry and Biophysics* **296** (1992), 426–434.

[75] OVANESOV, M. V., ANANYEVA, N. M., PANTELEEV, M. A., ATAULLAKHANOV, F. I., & SAENKO, E. L. Initiation and propagation of coagulation from tissue factor-bearing cell monolayers to plasma: initiator cells do not regulate spatial growth rate. *Journal of Thrombosis and Haemostasis* **3** (2005), 321–331.

[76] OVANESOV, M. V., KRASOTKINA, J. V., ULYANOVA, L. I., ABUSHINOVA, K. V., PLYUSHCH, O. P., DOMOGATSKII, S. P., VOROBEV, A. I., & ATAULLAKHANOV, F. I. Hemophilia a and b are associated with abnormal spatial dynamics of clot growth. *Biochimica Biophysica Acta (General Subjects)* **1572** (2002), 45–57.

[77] PHILLIPS, W. M., & DEUTSCH, S. Toward a constitutive equation for blood. *Biorheology* **12** (1975), 383–389.

[78] PIPKIN, A. C. *Lectures on Viscoelasticity Theory.* Springer Verlag, New York (1972).

[79] QUEMADA, D. A nonlinear maxwell model of bio-fluids application to normal blood. *Biorheology* **30** (1993), 253–265.

[80] RAJAGOPAL, K. R. Multiple configurations in continuum mechanics. Report Volume 6, Institute for Computational and Applied Mechanics, University of Pittsburgh, Pittsburgh, PA, 1995.

[81] RAJAGOPAL, K. R., & SRINIVASA, A. R. A thermodynamic framework for rate type fluid models. *Journal of Non-Newtonian Fluid Mechanics* **88** (2000), 207–227.

[82] RAJAGOPAL, K. R., & TAO, L. Modeling of the microwave drying process of aqueous dielectrics. *ZAMP* **53** (2002), 923–948.

[83] RAWALASHEIKH, R., AHMED, S. S., ASHBY, B., & WALSH, P. N. Kinetics of coagulation factor X activation by platelet-bound factor IXa. *Biochemistry* **29** (1990), 2606–2611.

[84] RIHA, P., LIAO, F., & STOLTZ, J. F. Effect of fibrin polymerization on flow properties of coagulating blood. *Journal of Biological Physics* **23** (1997), 121–128.

[85] RIHA, P., WANG, X., LIAO, R., & STOLTZ, J. F. Elasticity and fracture strain of whole blood clots. *Clinical Hemorheology and Microcirculation* **21** (1999), 45–49.

[86] ROSING, J., TANS, G., GOVERS-RIEMSLAG, J. W. P., ZWAAL, R. F. A., & HEMKER, H. C. The role of phospholipids and factor Va in the prothrombinase complex. *Journal of Biological Chemistry* **255** (1980), 274–283.

[87] SAKHAROV, D. V., NAGELKERKE, F. J., & RIJKEN, D. C. Rearrangements of the fibrin network and spatial distribution of fibrinolytic components during plasma clot lysis. *Journal of Biological Chemistry* **271** (1996), 2133–2138.

[88] SANTORO, S. A., & EBY, C. S. Laboratory evaluations of hemostatic disorders. In: R. Hoffman, E. J. Benz, S. J. Shattil, B. Furie, H. J. Cohen, L. E. Silberstein, and M. P., (eds), *Hematology : Basic principles and practice*, 3rd ed. pp. 1841–1850. Churchill Livingstone, Philadelphia (2000).

[89] SCHMIDSCHÖNBEIN, G. W., SUNG PAUL, K. L., TÖZEREN, H., SKALAK, R., & CHIEN, S. Passive mechanical properties of human leukocytes. *Biophysical Journal* **36** (1981), 243–256.

[90] SCOTT, C. F., SCHAPIRA, M., JAMES, H. L., COHEN, A. B., & COLMAN, R. W. Inactivation of factor XIa by plasma protease inhibitors. *Journal of Clinical Investigation* **69** (1982), 844–852.

[91] SHARP, M. K., THURSTON, G. B., & MOORE, J. E. The effect of blood viscoelasticity on pulastile flow in stationary and axially moving tubes. *Biorheology* **33** (1996), 185–206.

[92] SOLYMOSS, S., TUCKER, M. M., & TRACY, P. B. Kinetics of inactivation of membrane-bound factor va by activated protein c. *Journal of Biological Chemistry* **263** (1988), 14884–14890.

[93] SORENSEN, E. N., BURGREEN, G. W., WAGNER, W. R., & ANTAKI, J. F. Computational simulation of platelet deposition and activation: I. model development and properties. *Annals of Biomedical Engineering* **27** (1999), 436–448.

[94] SUN, N., & DEKEE, D. Simple shear, hysteresis and yield stress in biofluids. *Canadian Journal of Chemical Engineering* **79** (2001), 36–41.

[95] SUN, Y., & GAILANI, D. Identification of a factor IX binding site on the third apple domain of activated factor XI. *Journal of Biological Chemistry* **271** (1996), 29023–29028.

[96] THURSTON, G. B. Viscoelasticity of human blood. *Biophysical Journal* **12** (1972), 1205–1217.

[97] THURSTON, G. B. Frequency and shear rate dependence of viscoelasticity of blood. *Biorheology* **10** (1973), 375–381.

[98] THURSTON, G. B. Elastic effects in pulsatile blood flow. *Microvascular Research* **9** (1975), 145–157.

[99] THURSTON, G. B. The effects of frequency of oscillatory flow on the impedance of rigid blood filled tubes. *Biorheology* **13** (1976), 191–199.

[100] THURSTON, G. B. Rheological parameters for the viscosity, viscoelasticity and thixotropy of blood. *Biorheology* **16** (1979), 149–162.

[101] THURSTON, G. B. Light transmission through blood in oscillatory flow. *Biorheology* **27** (1990), 685–700.

[102] THURSTON, G. B. Non-newtonian viscosity of human blood: Flow-induced changes in microstructure. *Biorheology* **31** (1994), 179–192.

[103] THURSTON, G. B., & HENDERSON, N. M. A new method for the analysis of blood and plasma coagulation. *Biomedical Sciences Instrumentation* **29** (1993), 95–102.

[104] THURSTON, G. B., & HENDERSON, N. M. Impedance of a fibrin clot in a cylindrical tube - relation to clot permeability and viscoelasticity. *Biorheology* **32** (1995), 503–520.

[105] TROWBRIDGE, E. A. Mathematical concepts of blood flow and blood rheology. *Life Support Systems* **2** (1984), 25–38.

[106] TSCHOPP, T. B., BAUMGARTNER, H. R., SILBERBAUER, K., & SINZINGER, H. Platelet adhesion and platelet thrombus formation on subendothelium of human arteries and veins exposed to flowing blood in vitro - comparison with rabbit aorta. *Haemostasis* **8** (1979), 19–29.

[107] TSIANG, M., PABORSKY, L. R., LI, W. X., JAIN, A. K., MAO, C. T., DUNN, K. E., LEE, D. W., MATSUMURA, S. Y., MATTEUCCI, M. D., COUTRE, S. E., LEUNG, L. L. K., & GIBBS, C. S. Protein engineering thrombin for optimal specificity and potency of anticoagulant activity in vivo. *Biochemistry* **35** (1996), 16449–16457.

[108] TURING, A. M. The chemical basis of morphogenesis. *Philosophical transaction of the Royal Society of London. Series B, Biological Sciences* **237** (1952), 37–72.

[109] TURITTO, V. T., & BAUMGARTNER, H. R. Platelet interaction with subendothelium in flowing rabbit blood: Effect of blood shear rate. *Microvascular Research* **17** (1979), 38–54.

[110] TURITTO, V. T., & HALL, C. L. Mechanical factors affecting hemostasis and thrombosis. *Thrombosis Research* **92** (1998), S25–S31.

[111] TURITTO, V. T., WEISS, H. J., & BAUMGARTNER, H. R. The effect of shear

rate on platelet interaction with subendothelium exposed to citrated human blood. *Microvascular Research* **19** (1980), 352–365.

[112] USAMI, S., KING, R. G., CHIEN, S., SKALAK, R., HUANG, C. R., & COPLEY, A. L. Microcinephotographic studies on red cell aggregation in steady and oscillatory shear - a note. *Biorheology* **12** (1975), 323–325.

[113] VIRCHOW, R. *Über den faserstoff*: V. phlogose und thrombose im gefäßsystem. 1 ed. p. 458ff. Verlag v. Meidinger, Sohn and Corp., Frankfurt am Main (1856).

[114] VLASTOS, G., LERCHE, D., & KOCH, B. The superimposition of steady and oscillatory shear and its effect on the viscoelasticity of human blood and a blood-like model fluid. *Biorheology* **34** (1997), 19–36.

[115] VLASTOS, G., LERCHE, D., KOCH, B., SAMBA, O., & POHL, M. The effect of parallel combined steady and oscillatory shear flows on blood and polymer solutions. *Rheologica Acta* **36** (1997), 160–172.

[116] WALBURN, F. J., & SCHNECK, D. J. A constitutive model for whole human blood. *Biorheology* **13** (1976), 201–210.

[117] WALTERS, K., & KEMP, R. A. On the use of a rheogoniometer. part ii: Oscillatory shear. In *Polymer Systems : Deformation and Flow* (London, 1968), R. E. Welton and R. W. Whorlow, (eds), , British Society of Rheology, Macmillan, pp. 237–250.

[118] WHORLOW, R. W. *Rheological Techniques*. Ellis Horwood Ltd., Chichester (1980).

[119] WIEBE, E. M., STAFFORD, A. R., FREDENBURGH, J. C., & WEITZ, J. I. Mechanism of catalysis of inhibition of factor IXa by antithrombin in the pres-

ence of heparin or pentasaccharide. *Journal of Biological Chemistry* **278** (2003), 35767–35774.

[120] WURZINGER, L. J. Histophysiology of the circulating platelet. vol. 120. Springer-Verlag (1990).

[121] WURZINGER, L. J., OPITZ, R., WOLF, M., & SCHMID SCHÖNBEIN, H. Shear induced platelet activation - a critical reappraisal. *Biorheology* **22** (1985), 399–413.

[122] YELESWARAPU, K. K. *Evaluation of Continuum Models for Characterising the Constitutive Behavior of Blood.* PhD Dissertation, University of Pittsburgh, Pittsburgh, PA, 1996.

[123] YELESWARAPU, K. K., ANTAKI, J. F., KAMENEVA, M. V., & RAJAGOPAL, K. R. A mathematical model for shear-induced hemolysis. *Artificial Organs* **19** (1995), 576–582.

[124] YELESWARAPU, K. K., KAMENEVA, M. V., ANTAKI, J. F., & RAJAGOPAL, K. R. The flow of blood in tubes: Theory and experiment. *Mechanics Research Communications* **25** (1998), 257–262.

[125] YOUNG, M. E., CARROAD, P. A., & BELL, R. L. Estimation of diffusion coefficients of proteins. *Biotechnology and Bioengineering* **22** (1980), 947–955.

[126] ZARNITSINA, V. I., POKHILKO, A. V., & ATAULLAKHANOV, F. I. A mathematical model for the spatio-temporal dynamics of intrinsic pathway of blood coagulation. I. The model description. *Thrombosis Research* **84** (1996), 225–236.

VITA

Anand Mohan was born at Madras, India, and underwent his schooling at Padma Seshadri Bala Bhavan. He left school on a pleasant note, being selected as the Best Graduating Student of his class (1995), and being admitted through the portals of the Indian Institute of Technology (Madras). A fun-filled, unremarkable, and, in some ways, important four years later, he received the B.Tech. in Chemical Engineering. He arrived in the United States in the fall of 1999, and obtained his M.S. in Mechanical Engineering from Texas A&M University in 2001. He received his doctorate in Mechanical Engineering in August 2005, after a very productive and intellectually satisfying four years.

His permanent address is :

c/o Mrs. & Mr. S. Mohan,

18/4, Indira Colony,

First Avenue, Ashok Nagar,

Chennai - 600 083,

Tamil Nadu, India.